6

A Multi Finger Electromagnetic Actuator Apparatus for Biomechanical Studies on the Hand

by
Kathleen L. Dobson

B.S. Mechanical Engineering
Massachusetts Institute of Technology, 2003

SUBMITTED TO THE DEPARTMENT OF MECHANICAL ENGINEERING IN PARTIAL FULFILLMENT OF THE REQUIREMENTS FOR THE DEGREE OF

MASTER OF SCIENCE IN MECHANICAL ENGINEERING

AT THE
MASSACHUSETTS INSTITUTE OF TECHNOLOGY

JUNE 2005

©2005 Massachusetts Institute of Technology. All rights reserved.

Signature of Author: _____
Department of Mechanical Engineering
May 10, 2005

Certified by: _____
Lynette A. Jones
Principal Research Scientist in Mechanical Engineering
Thesis Supervisor

Accepted by: _____
Lallit Anand
Chairman, Department Committee on Graduate Students

MASSACHUSETTS INSTITUTE OF TECHNOLOGY
NOV 07 2005
LIBRARIES

BARKER

A Multi Finger Electromagnetic Actuator Apparatus for Biomechanical Studies on the Hand

by
Kathleen L. Dobson

Submitted to the Department of Mechanical Engineering on May 10, 2005 in Partial Fulfillment of the Requirements for the Degree of Master of Science in Mechanical Engineering

ABSTRACT

The focus of this thesis was on the design and construction of a multi-finger haptic device powered by electromechanical voice-coil actuators. Five actuators were designed and constructed and a position and force feedback control system was implemented for each. The maximum continuous force output for each actuator ranged from 12-16 N, which is about 15%-30% of the maximum force that can be exerted by an individual finger. The bandwidth of the controlled actuators ranged from 0.7 Hz to 1.7 Hz, the steady-state error was zero, and the overshoot ranged from 3.5% to 7.7%. Four actuators were constructed into an array, with finger contact points 23 mm apart. Additional structures, such as finger holders and a wrist rest, were developed to complete the human interface. With further modifications, the multi-finger apparatus can be used to conduct biomechanical and perceptual studies of the human hand.

Thesis Supervisor: Lynette A. Jones
Title: Principal Research Scientist in Mechanical Engineering

Acknowledgements

I would first like to thank my thesis advisor, Dr. Lynette Jones, for her patience and guidance over the past two years. She gave me a greater perspective on the importance of good research and provided me with the opportunity to explore ideas that I was not exposed to as an undergraduate. This project would not have been possible without her expertise on the hand and haptic devices, as well as her careful editing of this thesis.

I would also like to thank everyone in the BioInstrumentation lab for their help: Professor Ian Hunter for providing us with the lab's immense resources and his technical knowledge; Andrew Taberner for providing solutions to a range of engineering problems; Bryan Crane, Ariel Herrmann, Jordan Brayanov, and Mike Del Zio for their help with machining; Brett Lockyer for his electronics help and good conversation; Cathy Hogan and Nate Vandesteeg for their chemical safety help; and Kate Melvin for her administrative help. I am also indebted to James Tangorra, who was able to help me with almost any engineering problem, or point me in the right direction, and helped shape my ideas in the past two years. I am grateful for the opportunity to work in a lab with so many resources and so many talented scientists and engineers.

I would also like to thank Tom for his support, encouragement, and providing ideas when I was stuck. Finally, I want to thank my Mom and Dad for their support, love, and for believing in me.

This research was funded by the National Institute of Neurological Disorders and Stroke of the National Institute of Health (NS40836).

Table of Contents

List of Tables

List of Figures

1 Introduction

The focus of this thesis is on the design and construction of a multi-finger apparatus powered by electromechanical voice-coil actuators. The apparatus is to be used to perform studies on the human hand.

A better understanding of the function of the human hand is useful in order to reduce the occurrences of overuse hand and wrist injuries, such as carpal tunnel syndrome, improve hand surgery and rehabilitation, and provide insights that assist in the design of dexterous robotic hands. Previous areas of study on the human hand have included force characterization (e.g. Mathiowetz et al., 1985), force and position coupling (e.g. Ohtsuki, 1981; Hager-Ross et al., 2000), and dynamic response and characterization (e.g. Becker & Mote, 1990; Hajian & Howe, 1997). The purpose of this apparatus is to study the biomechanical, sensory, and functional aspects of hand use.

The apparatus developed is a haptic device, in which forces are delivered to the fingers resulting in a change in finger position. Computer-user interfaces for virtual reality applications, such as joysticks and gloves are the most common forms of haptic devices. Other applications of haptic devices include medical applications and remote handling of materials. Chapter 3 discusses several examples of these devices. Haptic devices have also been used to study hand function which is the objective of the apparatus described in this thesis.

Electromechanical voice-coil actuators were selected for this apparatus to apply forces to the hand. Voice-coil actuators were chosen because they can be designed to have low friction, low inertia, a high bandwidth, and are easily maintained, powered and controlled. The actuators consisted of flat copper magnet wire wound into a coil and

embedded into a fiberglass rotor. The rotor moves within an aluminum housing in which embedded neodymium rare earth magnets create a magnetic field of up to 3 T.

The multi-finger apparatus was designed to be capable of position control, through a closed-loop system, and force control, through an open-loop system. An optical system consisting of a laser diode light source and position sensor detector was used to sense the angular position of the rotor. A Proportional-plus-Integral-plus-Derivative (PID) controller was designed for each actuator to control its angular position. The controller was implemented using LabView. An open-loop force control system was also implemented in which the optical system was used to measure position and the force output was varied by changing the input current to the coils. The controlled actuators had smaller overshoot errors, slightly lower steady-state settling times and no steady-state error.

Improvements that could be made to the design include replacing the copper wire with lower weight aluminum wire, increasing the width between the magnetic housing to reduce rotor rubbing and friction, and altering the arrangement of wires attached to the rotors, to reduce damping. With these and other improvements, the apparatus will be a promising tool studies of the human hand.

2 The Hand

The human hand is a complex mechanical system. It consists of 27 bones and the 29 muscles that are located within the hand and forearm control its movements. A complicated feedback system is also required to control simultaneously the 21 degrees of freedom of movement in the hand and wrist (Jones & Lederman, in press).

For humans, the hands are used most often to grasp objects, an ability found only in mammals (Schieber & Santello, 2004). Grasping movements, which usually involve the entire hand, are limited in precision and accuracy (Jones, 1997). The most complex manipulative motions that human hands are capable of are evident in such tasks as watch-making, microelectronic assembly, and microsurgery (Jones, 1997). Other more common activities, such as typing and piano playing, require dexterity for quick and coordinated movements. Although motions such as typing require low force exertion, around 2.54 N at the fingertip (Martin et al., 1996), velocities of the fingertips can reach up to 800 deg/s at the fingertip (Gordon et al., 1994), with skilled typists typically performing up to 200,000 keystrokes per day (Martin et al., 1996). Similarly, pianists can average a keystroke every 56 ms (Shaffer 1982).

A better understanding of the biomechanics and dynamics of the hand is useful for many reasons. Overuse of the hand and wrist, as well as sub-optimal ergonomic design of human interfaces, has led to hundreds of thousands of work-related injuries per year (National Center for Health Statistics, 1994). One common type of musculoskeletal disorder is carpal tunnel syndrome, a repetitive strain injury of the wrist which currently affects over eight million Americans (Bureau of Labor and Statistics and National Institute for Occupational Safety and Health, 2002). Carpal tunnel syndrome, which

affects the tendons passing through the carpal bones in the wrist, is commonly caused by small precision movements performed at high speeds, such as typing. More ergonomic keyboards have been developed in an attempt to reduce the occurrence of repetitive strain injuries.

An understanding of the biomechanics of the hand is also useful in order to improve hand surgery and rehabilitation for functional recovery after hand reattachment, transplantation surgery or after-stroke therapy (Schieber & Santello, 2004). In addition, an understanding may provide insights that assist in the design more dexterous robotic hands.

2.1 Anatomical Structure

2.1.1 Bones

There are 27 bones in the hand: 8 in the wrist, 5 in the palm, and 14 in the fingers. The five bones in the palm, each connected to a digit, are the metacarpals. Each finger has three phalanges. From the palm to the finger tips, they are the proximal phalanx, middle phalanx, and dorsal phalanx. The thumb has only two phalanges. Each finger has three joints: the metacarpophalangeal (MP) joint is located between the metacarpals and the proximal phalanx, or at the finger's knuckle; the proximal interphalangeal (PIP) joint is between the proximal phalanx and the middle phalanx, and the distal interphalangeal (DIP) joint is between the middle and distal phalanges. Each joint has a different range of flexion: 85 degrees for the MP joint, 110 for the PIP joint, and 65 degrees for the DIP joint (Jones & Ledermann, in press).

2.1.2 Muscles

The muscles that control the movements of the hand can be divided into two main groups: extrinsic muscles, which take their origin in the forearm, and intrinsic muscles, which are located entirely within the hand. Extrinsic muscles control the flexion and extension of the hand and wrist (Jones, 1997). The three main extrinsic muscles for the fingers are the flexor digitorum profundus (FDP), the flexor digitorum superficialis (FDS) and the extensor digitorum communis (EDC). The FDS contributes to the flexion of the PIP joints of the fingers, especially when the wrist is flexed. The muscle is located more superficially than the FDP and is used more often for hand movements that require power. The FDP contributes to the flexion of the PIP joints, the MP joints, and the wrist joints and is the only muscle responsible for the flexion of the DIP joints. The EDC extends the MP joint and contributes to the extension of the PIP and DIP joints (Tubiana, 1981).

Intrinsic muscles control adduction/abduction movements of the fingers, the flexion of metacarpophalangeal joints, and the extension of the interphalangeal joints (Jones, 1997). The two main types of intrinsic muscles that control finger movements are the interossei and the lumbricals. The interossei are located between the metacarpals in the palm of the hand. The interossei are responsible for flexion of the MP joint and extension of the PIP and DIP joints. The muscles also contribute to abduction and adduction movements; the four dorsal interossei are responsible for abduction of the fingers while the three palmar interossei are responsible for adduction of the fingers. The lumbricals connect flexor tendons to extensor tendons and are unique in that they originate from tendons and not from bones. They are responsible for extension of the PIP

and DIP joints and flexion of the MP joints. Finally, the lumbricals of the index finger are more specialized than those of other fingers, as they play some role in the adduction and rotation of the finger (Tubiana, 1981).

2.2 Maximum Force Exertion

The maximum forces that can be exerted by human fingers depend on the type of grasp used. Power grasps, which involve the entire hand including the palm, have high stability and force while precision grasps, which only involve the fingertips, are less powerful but more dexterous (Burdea, 1996). Mathiowetz et al. (1985) measured the hand strength of 310 male and 328 female adults for four different grips. As shown in Table 1, the average maximum power grip strength for their male test subjects (ages 20-49) was measured to be 526 N and for their female test subjects (ages 20-49) was 319 N. For more precise grips, such as the tip pinch, key pinch, and palmar pinch, the maximum force that could be exerted by both men and women was lower. By comparison, Westling and Johansson (1987) found that the typical forces exerted for grasping and precision manipulation are around 2 N.

Table 1. Average performance of 20-49 year olds in different grasps, right hand only (adopted from Mathiowetz et al., 1985).

Grasp	Description	Men	Women
Grip Strength	Power grip with entire hand	526 N	319 N
Tip Pinch	Thumb tip to index fingertip	80.4 N	53.3 N
Key Pinch	Thumb pad to lateral surface of index finger	116 N	77.8 N
Palmar Pinch	Thumb pad to pads of index and middle fingers	113 N	79 N

The maximum force that an individual finger can exert has been found to be dependent on the number of other fingers active at the same time. Ohtsuki (1981) found that fingers were capable of exerting their maximum strength when acting alone, and that as the number of fingers being flexed increased, the force exerted by each finger decreased. The decline in strength of the middle and index fingers when they were flexed with other fingers was about 30% whereas the decrease in the ring and little fingers was 15-25%. The total grip strength of all four fingers is only about 75% of the sum of each individual finger acting alone (Ohtsuki, 1981). Ohtsuki reasoned that the cause of this decrease during simultaneous flexion had a neurophysiological origin rather than a biomechanical origin, but the exact cause is still subject to debate.

Finally, the relative contribution of individual fingers to the total force exerted varied with the largest contribution from the middle finger, at 33%, and the smallest from the little finger, at 15%. Ohtsuki attributed this distribution to the anatomical arrangement of bones in the hand, where the middle finger sits along the same axis as the capitate bone in the wrist and the radius in the forearm.

2.3 Coupling of Finger Movements

Individual fingers do not move entirely independently of each other. When a single finger is flexed, there is an unintentional flexion of additional fingers or joints. This coupling is a result of both biomechanical and neural factors.

2.3.1 Biomechanical constraints

There are many sources of mechanical coupling in the hand and the resulting interdependence of the movement of the fingers is well known. This mechanical

coupling originates from passive connections, such as soft tissue, interconnections between tendons, and some multitendoned extrinsic muscles acting on more than one digit.

The three major extrinsic muscles, the FDP, FDS, and ED, are compartmentalized into four sections, each corresponding to a different finger. The tendons of each compartment attach to each of the four fingers. When a multi-tendoned muscle is activated more than one finger may flex, due to this mechanical coupling. In the past, the FDP has been assumed to be compartmentalized such that for each finger flexed, a different section of muscle is activated. However, EMG activity recorded during flexion and extension of each individual finger has shown incomplete subdivisions within the FDP coupled with specialized functional regions (Reilly and Schieber, 2003). Kilbreath et al. (2002) found that the FDP is compartmentalized such that single motor units allow for selective control of forces at the tips of the index, middle, and ring fingers in a grasping orientation; that is the flexion of one finger resulted in less than a 20% increase in exerted force for the other fingers. Flexion of the little finger, however, resulted in a mean change in the force exerted by the ring finger of 62% (Kilbreath et al., 2002). The EDC similarly gives rise to multiple tendons that insert into all four fingers, which results in mechanical coupling when fingers are extended. However, by stimulating the EDC muscle fibers and measuring the force produced at the finger tips, Keen and Fuglevand (2003) concluded that these linkages play only a minor role in finger coupling.

The interconnection of tendons also contributes to mechanical coupling in the hand. One such web of interconnecting tendons arises from the FDP. Thin sheets of inelastic tissue, as well as the origins of the lumbrical muscles, interconnect the tendons

in the palm of the hand (Schieber & Santello, 2004). Also, strong tendon connections between the middle and little fingers arise in the lower third of the forearm (Tubiana, 1981).

2.3.2 Independence of fingers

The extent of coupling between different fingers has been quantified in several studies. Zatsiorsky et al., (1998) found that actively flexing one digit resulted in other nonactive digits exerting between 2 and 52% of the force of the active digit. Hager-Ross and Schieber (2000) found no difference in the extent of coupling between dominant and non-dominant hands.

Hager-Ross and Schieber (2000) characterized the independence of the fingers by recording the motion of all the digits when subjects were instructed to move just one digit. The motion was recorded using both a video motion analysis system and an instrumented glove. They found that the index finger is the most independent of the fingers, followed by the little finger, middle finger, and ring finger. Other experiments give additional supporting evidence that the middle and ring fingers are less independent in both flexion and extension. For example, when the middle finger is fully extended, 41% of people cannot flex the DIP joint of their ring finger and 11% of people cannot flex the DIP joint of their extended little finger (Tubiana, 1981). The little finger is capable of more independent movement than either the ring or middle finger, however, independent movement is rarely required for the little finger in everyday tasks.

2.3.3 Neurophysiological coupling and control

Coupling between the fingers also arises when two or more muscles have common neural inputs. These inputs can cause several muscles to contract when a signal is sent down to motorneurons that control more than one muscle. This may lead to synchronized contractions in one muscle or the muscles of one finger. Reilly and Schieber (2003) found that motor units of fingers adjacent to one being flexed will discharge in order to stabilize them and prevent them from flexing. This is consistent with Ohtsuki (1981) who found a reduction in the maximum strength of fingers when flexed together as compared to when they are flexed independently. He hypothesized that the source of this reduction was from the motor cortex.

2.4 Dynamic Response of fingers

In addition to studying the coupling of the fingers, the object of the apparatus being built is to also study the dynamic response of the fingers to external forces. Hajian and Howe (1997) measured the mechanical impedance of the human finger primarily by rotating the MP joint. In the study, a position impulse was applied to a finger flexed at a given force ranging from 2 N to 20 N, and the position and force response was measured. The data were fit to a second-order model. The values for the mass, damping and stiffness varied depending on the force level of the finger. The stiffness of the finger increased as the force level of the fingertip increased, from about 200 N/m for 2 N force level to about 800 N/m for the 20 N force level. The damping also increased with force level, from about 2.2 Ns/m to about 4 Ns/m. The equivalent mass of the finger remained unchanged with the change in force. Becker and Mote (1990) also measured the mechanical impedance of human fingers about the metacarpophalangeal joint but with abductive-

adductive rotation. They found this system can also be modeled as a linear, second order, damped oscillator with the stiffness and damping coefficients increasing with isometric muscle contraction and hence force level. Becker and Mote also observed that muscle fatigue caused the stiffness and damping parameters to increase.

Shimoga (1992) characterized the sensing and control bandwidth of the human finger. Although tactile signals can be sensed by human fingertips up to a bandwidth of 1000 Hz, the human finger can not comfortably apply force commands at a bandwidth higher than 5 to 10 Hz. Shimoga also found that human fingers cannot react to unexpected force or position signals at a bandwidth higher than 1 to 2 Hz. Kunesch et al. (1989) found that rapid finger and hand movements, such as those involved in typing and tapping, are typically performed at frequencies of 4 to 7 Hz.

2.5 Summary

Studies of the human hand have resulted in numerous characterizations such as the maximum force exertion of the fingers acting independently and together, the extent of coupling between fingers, and the dynamic response of fingers. It has been shown that individual fingers do not act entirely independently; the force that each finger can exert and the range and velocity of motion of one finger is dependent on the action of the other fingers. Still subject to debate is the extent to which this coupling can be attributed to biomechanical and neurophysiological sources. The purpose of the multi-finger apparatus is to further explore position and force coupling and to gain a better understanding of the source of this coupling.

3 Haptic Displays and Actuator Technology

3.1 Design goals

The apparatus was developed to study a number of aspects of manual function including biomechanics, finger movement control, and haptic perception in the hand. In order to study all the fingers, the apparatus needed to have a number of actuators. These actuators needed to be compact, so that they could fit the geometry of the hand, yet powerful, delivering up to 40 N to the fingertip of a subject. In order to mimic the anatomical rotation of a finger about the metacarpophalangeal joint, a rotary actuator, as opposed to a linear actuator, was required. The desired range of motion for rotation of the actuator needed to approach that of the finger about the MCP joint, which is about 90 degrees. In order to match the maximum bandwidth with which the human finger can move comfortably, the apparatus needed to have a bandwidth of at least 7 Hz (Kunesch et al., 1989). Finally, both the force exerted on the fingertip and the position of the actuator had to be controlled by a feedback system.

3.2 Actuator Technology

Actuators are used to transmit force. A wide range of actuator technology exists that exhibits a variety of characteristics. The most commonly used actuators are electrical, pneumatic, and hydraulic. Other actuators, such as electrochemical and piezoelectric, are less common but often have unique and desirable characteristics for specific applications.

3.2.1 Hydraulic actuators

Hydraulic actuators translate forces through the flow of fluid and can be either rotary or linear. Because of the incompressibility of the hydraulic fluid, which is usually oil, hydraulic actuators are capable of rapid responses and have a high bandwidth. Also, high fluid pressure enables hydraulic actuators to have high output forces (Burdea, 1996). However, there are drawbacks to hydraulic actuators. Because they need to handle high fluid pressure, the actuators are usually heavy and bulky. They are also more difficult to use than other actuators, mainly because the working fluid needs to be controlled and filtered. Finally, there is a danger of the actuators overheating (Kato & Sadamoto, 1987).

3.2.2 Pneumatic actuators

Pneumatic actuators transmit force by compressing air. They are widely used for linear applications. The output force of pneumatic actuators is a function of the pressure of air in the actuator. Because air is not capable of reaching as high a pressure as fluid, the maximum force of pneumatic actuators is lower than that for hydraulic actuators. Also, the response time is slower, since it takes four times longer for waves to propogate in air than oil (Burdea, 1996). Despite the safety, ease of use, and low cost of pneumatic actuators, they are often bulky and their power-to-weight ratio is lower than that for hydraulic actuators.

3.2.3 Electrical actuators

Electrical actuators translate electricity into a mechanical force by altering a current through a magnetic field. An advantage of electrical actuators is that their source of power, electricity, is very accessible. Also, they are safe, easy to use, and, though they

do not have as high output power as hydraulic actuators, their power-to-size ratio can be very low. A variety of electrical actuators exist that have a range of sizes, maximum forces, and speeds. These include direct-current motors, solenoids, and electromagnetic coil actuators.

3.2.3.1 Direct-Current Motors

Direct-current motors consist of a rotor surrounded by a stationary stator. Force is generated by the interaction of the magnetic fields of the rotor and stator. One, and sometimes both, of the magnetic fields of the rotor and stator are produced by controlling the current running through the coil. In this way, force output is a function of the input current.

Direct-current motors can be divided into two subgroups based on the composition of the rotor. Brush motors have field windings in the rotor and a DC power source connects to the field winding through brushes. In brushless motors, the rotor consists of a permanent magnet and, therefore, no electrical connections are needed between the power source and the rotor. Because the rotor has no electrical windings, brushless motors are smaller and have a faster response. However, brushless motors are often more expensive because they require additional sensing and control (Burdea, 1996).

3.2.3.2 Solenoids

In a solenoid, a tightly-wound wire creates a magnetic field which can be altered to move a magnetic plunger. Although most applications of solenoids are simple and require low positional accuracy, such as doorbells, solenoids can be very precisely controlled in

certain applications, such as speakers. Solenoids are linear actuators and have limited travel.

3.2.3.3 Moving coil actuators

A moving coil actuator consists of a rotor embedded with a wound coil and surrounded by a permanent magnet housing. Moving coil actuators are similar to brush motors except that the electrical connections to the rotor are permanent. Because of the permanent connections, the range of motion for a moving coil actuator is limited and the actuators can not continuously rotate. There are several advantages to moving coil actuators. They are compact in size, have a fast response time and are easier to control than DC motors. However, because of high currents that travel in the rotor wires, they are prone to overheating.

3.2.4 Other actuators

Electrochemical actuators are fabricated from materials that undergo a shape change when a voltage is applied across them. Electrochemical actuators include elastomers, conducting polymers, molecular actuators, and shape memory alloys. All of these materials change their shape with an applied voltage, and can be used as an actuator to produce a force. Although electrochemical actuators are reliable and accurate, they are generally slow and produce small movements.

Other types of actuators include piezoelectric and electrostatic. In piezoelectric actuators, a voltage is applied across a crystalline substance which results in a shape change. Although these actuators are very accurate, they produce small deformations. Electrostatic actuators, in which a diaphragm is moved by changing the electric field

between two stationary conductive panels, can only be used for applications on the sub millimeter scale.

3.3 Haptic Interfaces

Haptic interfaces are devices that transmit information to a human user, through the application of forces to the user's body, typically the hand. Actuators are used to transmit forces and force sensors are used to detect forces exerted by the user's body. Applications for haptic interfaces include computer-user interfaces in virtual reality applications, and remote control of robots such as in surgery or space.

3.3.1 Computer-user Interfaces

Force-feedback joysticks have also been used for many years for computer graphic, industrial and entertainment applications (Burdea, 1996). Examples of force-feedback joysticks include spherical joysticks, in which the handle rotates about a spherical joint, Cartesian joysticks, in which the handle can translate in two or three orthogonal directions, and platform joysticks, in which the handle rests on a moveable platform (Burdea, 1996). Joysticks are also commonly used for virtual reality applications.

3.3.2 Virtual Reality

Many types of haptic devices have been developed for virtual reality applications. These devices can be externally grounded to a desk, floor, ceiling or wall, or internally grounded to the user's body. Externally grounded devices are capable of greater forces and can be used to transmit the perception of weight. Body-grounded devices are more portable and allow a greater freedom of movement. Examples of externally grounded

haptic devices include pen-based masters, such as the PHANTOM (SensAble Technologies) and stringed interfaces, such as the SPIDAR (Ishii & Sato, 1994). Body-grounded devices include sensing gloves, such as the CyberGlove (Immersion Corporation), and force-feedback gloves, such as the Rutgers Master (Burdea et al., 1992).

3.3.2.1 Pen-based Masters

Pen-based masters are externally grounded devices that allow the user to interact with a virtual environment through a pen, pointer, or other familiar devices (Burdea, 1996). They are usually compact, have a larger workspace than joysticks, and can have between three and six degrees of freedom. Although the geometrically constant pen eliminates the need for complex calibrations, it also limits the experimental and modeling capabilities of the device, since information is only available about a specific point of contact.

An example of a pen-based master is the Personal Haptic Interface Mechanism (PHANTOM) Master (SensAble Technologies), shown in Figure 3-1, which is a force-feedback device that is used in a number of applications including haptic research, virtual reality, and computer-aided design. SensAble Technologies produces several models of the PHANTOM, which vary in their workspace, footprint, range of motion, and maximum force exertion. The PHANTOM Desktop Device is a force-feedback system with six degrees of freedom. It has a 160 mm by 120 mm by 120 mm workspace and is capable of 7.9 N maximum force output.

Figure 3-1. The PHANTOM Master Desktop Model, sold by SensAble Technologies, is a pen-based force-feedback device.
(http://www.sensable.com/images/products/Large%20PHANTOM%20Omni%20Image.jpg)

3.3.2.2 Stringed Force-Feedback Interfaces

Stringed force-feedback interfaces transmit forces to the fingertips using the tension of strings. Actuators are used to rotate pulleys which tense the strings. Although stringed force-feedback interfaces have large workspaces, low weight and low inertia, due to the light weight of strings, one significant drawback is that multiple fingered set-ups are difficult to use because the strings can tangle.

An example of a stringed force-feedback interface is the Space Interface Device for Artificial Reality (SPIDAR) (Ishii & Sato, 1994). The SPIDAR consists of four strings attached to a cap, in which the forefinger is placed. Each string goes to a separate corner of a cubic frame where it is wound around a pulley. The pulleys are controlled by electric motors. The fingertip position is measured by a rotary encoder on each motor, which senses the extension of the string. The SPIDAR is capable of three degrees of

freedom, has a workspace of 30 cm cubed, and each motor is capable of exerting up to 4 N.

3.3.2.3 Sensing and Force-Feedback Gloves

Gloves are often more maneuverable than stringed or pen-based masters. They can be used to take measurements and give force feedback to several fingers. Although gloves can be externally grounded, most gloves are grounded to the user's body, enabling a greater flexibility in hand movement.

The CyberGrasp Glove (Immersion Corporation) is a commercially available body-grounded glove that provides force feedback to a user's fingers. As shown in Figure 3-2, the five force actuators, one for each digit, run along the back of the user's hand. The position of the hand is measured by position sensors on the glove, and a control system enables the device to provide force-feedback. The glove has a one meter spherical radius workspace and each actuator can continuously exert up to 12 N of force on the user's fingers. Applications for the CyberGrasp Glove include virtual reality training and simulation, computer-aided design, remote handling of hazardous materials, and medical applications.

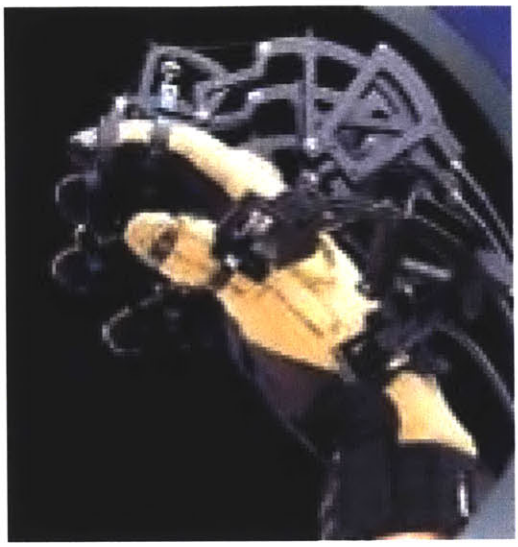

Figure 3-2. The CyberGrasp Glove, sold by Immersion Corporation, is a body-grounded force-feedback glove with an exoskeleton that runs along the back of the hand. (http://www.immersion.com/3d/docs/cybergrasp_datasheet.pdf)

The Rutgers Master (Burdea et al, 1992) is a body-grounded glove master with force-feedback. The Rutgers Master is used for virtual reality applications and biomechanical studies of the hand. Force is exerted at the tips of the thumb, index and middle digits by three pneumatic actuators, located within the palm of the hand. Each actuator is capable of up to 4 N of force. The actuators have a 50 to 100 ms rise time and a bandwidth of 10 to 20 Hz. It is a lightweight, portable device with a mass of 0.045 kg. Magnetic position sensors measure the palm position and orientation in space while optical sensors measure the finger angles of the operator's hand. Since it is a body-grounded device, the Rutgers Master is not able to simulate weight. The second generation glove, shown in Figure 3-3, contains an additional actuator acting on the ring finger. The second generation glove is also able to exert up to 16.4 N of force at the user's fingertips, has a 15 Hz bandwidth, and has a 50-90 degree flexion workspace (Gomez et al., 1994).

Figure 3-3. The second generation Rutgers Master is a body-grounded force-feedback device that uses pneumatic actuators to exert force at the fingertips.
(http://www.caip.rutgers.edu/vrlab/projects/rm2/system.html)

3.3.3 Studies of Human Hand Function

Many of the haptic devices described can be used to study the human hand. There are also several devices that have been developed exclusively for studies of human hand function. Haptic displays developed for this application are often simpler, in order to isolate specific physiological structures, or have different feedback systems.

Many haptic interfaces are force-feedback controlled. Although force-feedback is suitable for virtual reality applications, often times it is desirable to study and control the position of fingers. Positional displays require position sensors and a closed-loop position control system. An example of a position-controlled apparatus used for studies of the human hand is the Tactuator, developed by Tan et al. (1999). The purpose of this device was to study how quickly information could be processed by a subject's fingertips

only using tactile cues. The Tactuator is driven by three independent, one-degree-of-freedom disk-drive head-position motors. Three rods, one each for the thumb, index finger and middle finger, serve as the contact points for the fingers as shown in Figure 3-4. The range of motion of the device is a 25 mm line for each finger. Each actuator has a bandwidth of 300 Hz.

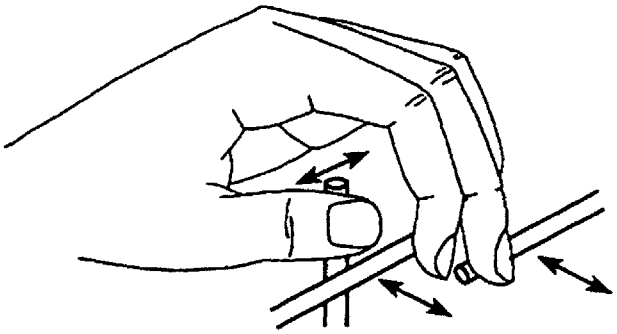

Figure 3-4. Schematic drawing of finger placements and trajectories for the Tactuator. (http://dynamo.ecn.purdue.edu/~hongtan/pubs/PDFfiles/J08_Tan_PP1999.pdf)

3.4 Applications of Electromagnetic Actuators for Haptic Displays

There are several examples of haptic displays that have used electromagnetic actuators to provide force feedback. Electromagnetic actuators have many characteristics that make them desirable for haptic applications such as quick response time, compact size, and output forces on the scale of the maximum forces fingertips are capable of exerting.

3.4.1 Multi-finger Moving Coil Actuator Haptic Display

The Fingertip Haptic Display (FHD), developed by Leuschke et al. (2005), is a multi-finger device that uses electromagnetic actuators to produce forces on the fingertips. The display contains four actuators, one for each finger, and each actuator consists of two flat

coils embedded in a moveable rotor surrounded by a permanent magnetic housing. The width of each actuator is 27 mm. The actuators have low inertia, low friction, and good heat dissipation. Attached to each actuator is a five-bar mechanism which contains a platform for the fingertip to rest. The motion of the platform is limited to a horizontal plane and the workspace of the device was designed to accommodate 95% of the human population in terms of flexion and extension movements of the fingers (Leuschke et al, 2005).

The FHD uses an optical system to sense both the position of the device and the direction of motion. The maximum continuous steady-state current that can be delivered to the device is 1.4 A which results in an output torque of 164 Nmm. The FHD can safely output peak torques of over 600 Nmm for brief periods of time. If the distance between the contact point and the center of the rotor is estimated to be about 100 mm, then the maximum continuous and peak force that can be exerted on the fingertip is 1.64 N and 6.00 N respectively.

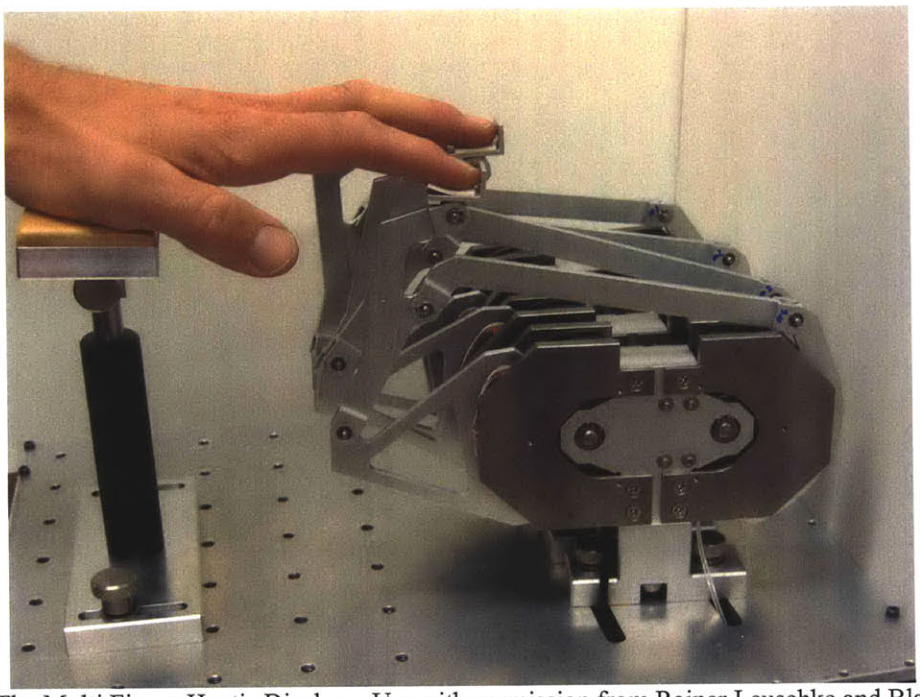

Figure 3-5. The Multi Finger Haptic Display. Use with permission from Rainer Leuschke and Blake Hannaford of University of Washington.

3.4.2 Virtual Piano Haptic Display

Gillespie and Cutkosky (1993, Gillespie 1994) used electromechanical voice-coil actuators to construct a single-key virtual piano haptic display. The purpose of the device was to improve the feel of a synthesizer keyboard so that it matched that of an acoustic piano. The device uses a force-feedback loop to control the response of the virtual piano key. The mechanical parameters of the virtual key, such as damping and stiffness, could be adjusted to better simulate an actual key.

3.4.3 Voice-coil Actuators for Automatic Piano

Hayashi et al. (1994, 1999) used electromechanical voice-coil actuators in the fabrication of an automatic piano. The objective of their research was to improve the performance of an automatic piano so that the sounds it produced were similar to those produced by pianists. A lightweight rotary actuator was used in the design. Aluminum flat wire was

wound into a coil which was then embedded into an epoxy resin laminated plate. The rotor was surrounded by a structure that housed rare-earth cobalt magnets, which resulted in a magnetic flux of 0.45 T in the 5 mm housing gap. The resulting actuator torque was 1.33 Nm/A and the maximum possible force that could be exerted at the point of contact was 13.3 Nm/A. (For 3.5 A of maximum continuously applied current, this results in a force of 46.55 N at the contact point.) The actuator was controlled by a position control loop. The position of the rotor was measured optically and the control system was implemented on a computer. The controlled actuator had a natural frequency of about 60 Hz.

3.5 Apparatus Overview

The apparatus constructed as part of this thesis is a modified version of the voice-coil actuators developed by Hayashi et al. (1994, 1999) and adapted for studies of the hand. Electromechanical voice-coil actuators were used because they have low inertia, low friction, and can have a quick response time. The bandwidth obtained by the actuators in Hayashi's automatic piano was 60 Hz, which is much greater than the bandwidth over which humans can control their fingers (i.e. around 7-10 Hz). The voice-coil actuators of the automatic piano were rotary, which is desirable for studying rotational movement about the MCP joint. Voice-coil actuators can be compact. The width of the actuators in the automatic piano was 23 mm which is 4 mm less than the width of the actuators used for the FHD. Finally, voice-coil actuators require lower maintenance than other types of actuators, such as hydraulics, and, despite the risk of overheating, are relatively safe.

In addition to having specifications that were desirable for human hand studies, the piano's actuators were capable of position-controlled movement. Optical sources and

sensors, which introduce no additional friction to the system, were shown to be effective and reliable. These actuators could also be used for force-feedback control, by opening the control loop.

There were several modifications made to the design of the piano's actuators in order to meet the objectives of the apparatus. The magnetic housing was modified in order to increase the range of motion and to provide a structure on which to rest the user's hand. The size and shape of the rotors were modified in order to fit into a housing and to provide keys on which the user's fingers could rest. Also, external structures were constructed to provide additional support for the user's hand and arm. Further discussion of these modifications, as well as other design considerations for the actuators and control system is presented in Chapters 4 and 5.

4 Design and Construction of Actuator

4.1 Electromagnetic Theory

The torques, forces, and movements produced by the electromagnetic actuators can be described from basic laws of electricity and magnetism. An electromagnetic force is exerted on a current-carrying wire running through a magnetic field. This force, F, is proportional to the length of the wire, L, the magnitude of the current, i, and the magnitude of the magnetic field, B, that is perpendicular to the direction of the wire:

$$F = i \cdot \vec{L} \times \vec{B} \tag{4.1}$$

If the wire is turned into a loop, then the electromagnetic force acts only on the part of the wire which is perpendicular to the magnetic field. In many electromagnetic actuator applications, including the one in this thesis, a loop of wire will be placed in two parallel magnetic fields running in opposite directions, as shown in Figure 4-1. In this arrangement, the force acting on the wire is proportional to the length of the wire, h_1 and h_2, in each magnetic field, B_1 and B_2:

$$F = i \cdot \vec{h}_1 \times \vec{B}_1 + i \cdot \vec{h}_2 \times \vec{B}_2 \tag{4.2}$$

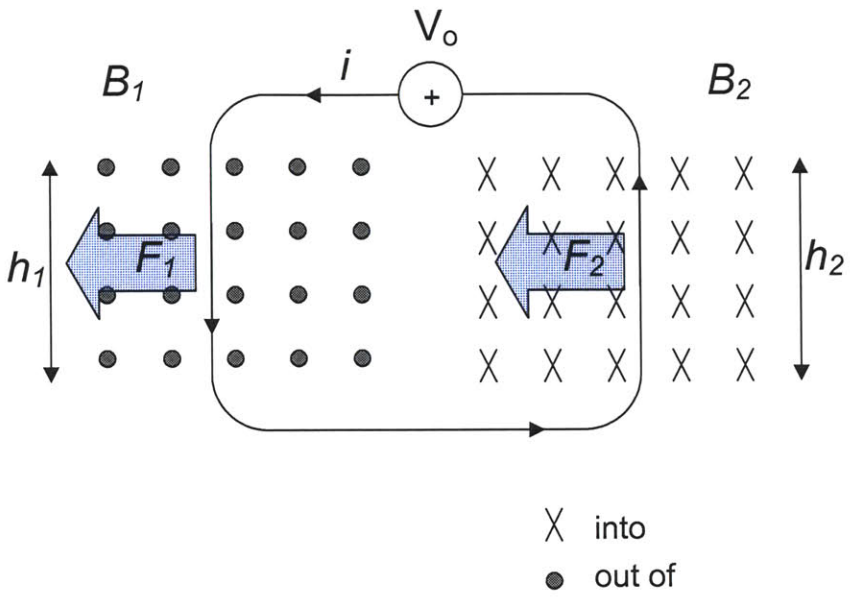

Figure 4-1. Forces, F_1 and F_2 acting on a current-carrying wire running through magnetic fields B_1 and B_2.

This electromagnetic effect can be multiplied when additional wires are placed in the magnetic field. For a coil of wire with n turns, the total force acting on the coil of wire is:

$$F = n \cdot (i \cdot \vec{h}_1 \times \vec{B}_1 + i \cdot \vec{h}_2 \times \vec{B}_2) . \tag{4.3}$$

The torque, τ, on the rotor is then the cross-product of the distance between the rotational axis and the acting force. Integrating this over the length of wire in the magnetic field results in the cross product between the net force on each wire and the average distance, d, of the wire from the rotor:

$$\tau = d \times F = d \times n \cdot (i \cdot \vec{h}_1 \times \vec{B}_1 + i \cdot \vec{h}_2 \times \vec{B}_2) \tag{4.4}$$

The resulting force, F_{result}, acting at a contact point a distance d_{result} from the rotational axis, as shown in Figure 4-2, is the torque on the rotor divided by d_{result}:

$$F_{result} = \frac{\tau}{d_{result}} = \frac{d}{d_{result}} \times n \cdot (i \cdot \vec{h}_1 \times \vec{B}_1 + i \cdot \vec{h}_2 \times \vec{B}_2) \tag{4.5}$$

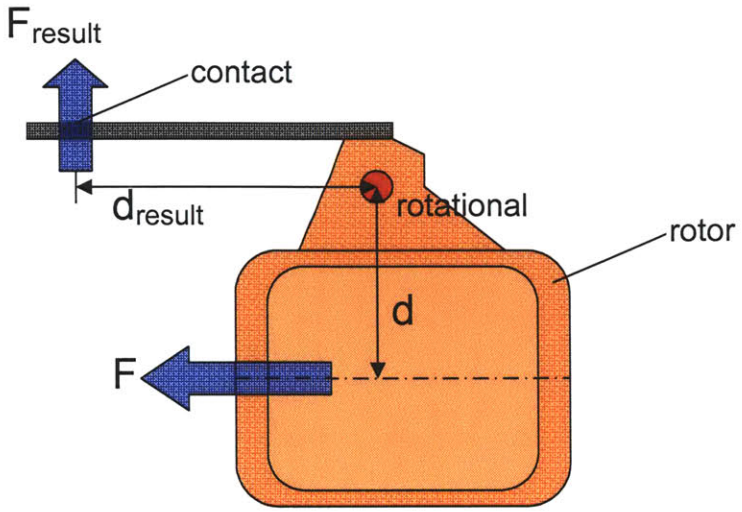

Figure 4-2. An electromagnetic force, F, acts on the rotor a distance d from the rotational axis to produce the resulting force F_{result} at a point a distance d_{result} from the rotational axis.

4.2 Actuator Design

The actuator design consisted of a lightweight rotor rotating between a stationary structure that produced two parallel but opposite magnetic fields, as illustrated in Figure 4-1. In addition, aluminum keys and finger holders were constructed so that the force generated by the rotor could be applied to or counteract the forces produced by the finger pad in contact with the key.

4.2.1 Rotor and coils

The rotor housings, designed and machined by Dr. Eiji Hayashi, were made from fiberglass. Fiberglass was chosen because it is a strong, yet lightweight material. The rotor axles were inserted into miniature steel bearings. Steel spring washers were placed between the ball bearings and the rotor fixtures on the walls to improve rotor movement.

The coils were made from copper magnet wire with a rectangular cross-section coated with a polyamideimide bondcoat (Alpha-Core, Inc). The wire used was 0.26 mm by 1.04 mm. The polyamideimide bondcoat, which functioned as an electrical insulator

as well as an adhesive, has a melting temperature of 220 °C. In order to wind the wire into coils, an aluminum rig was constructed (see Figure 4-3). The rig consisted of a trapezoidal-shaped core, onto which the wire was wound, surrounded by two circular plates which guided the wire so that it was wound into a flat coil. A cylindrical piece, attached to the top plate, provided a way to spin the assembly. The wire was wound using a milling machine (Dynamyte 1007). The cylindrical piece was clamped in a collet and spun slowly, about 1 rotation per second. Wire was fed into the rig from a large spool (see Figure 4-4). After the coils were spun, they were placed in an oven (Thermolyne 47900 furnace) at 230 °C. They were baked for 3 hours, cooled, and then removed from the rig. In the baking process, the polyamideimide coating bonded the wire into a flat, cohesive unit. Before the coils were affixed inside the rotors, their resistance was measured, in order to determine whether the oven curing process resulted in any short-circuits in the coils. The resistance of each coil is listed in Appendix A.

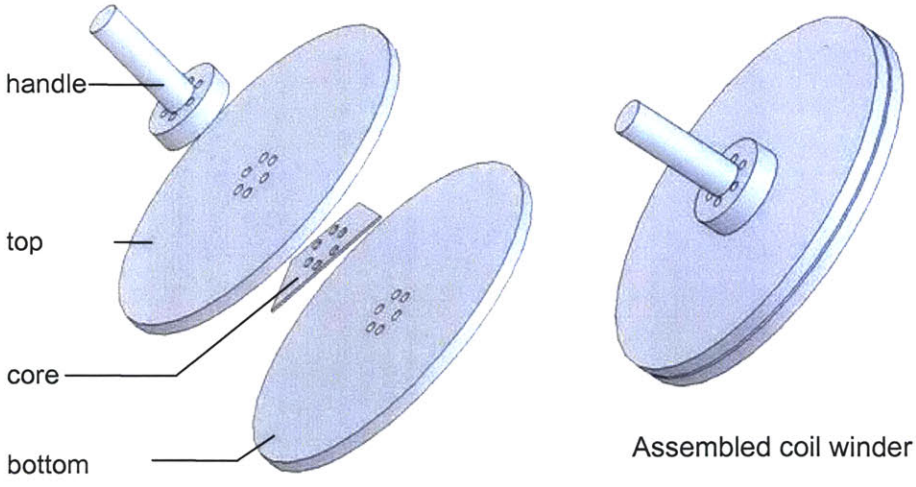

Figure 4-3. The aluminum rig constructed to wind the coils consisted of a handle, core and two plates.

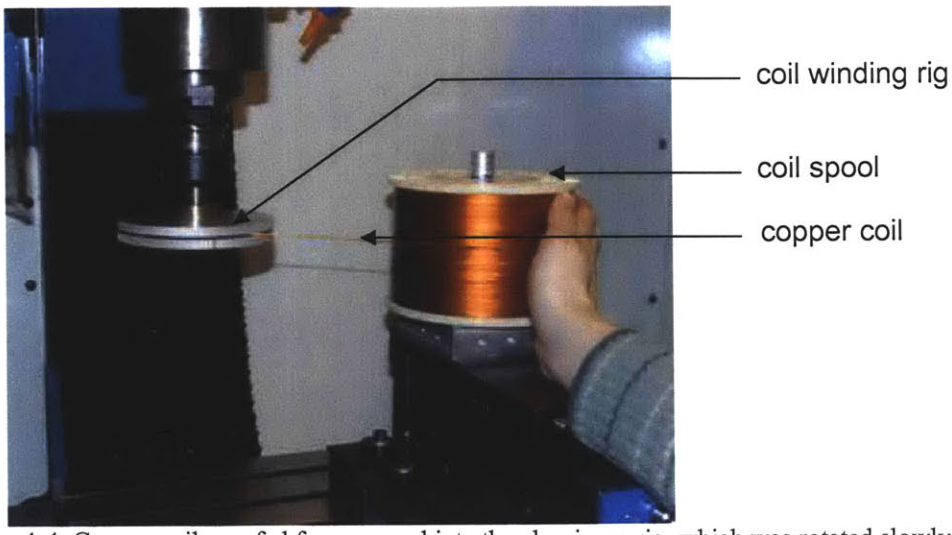

Figure 4-4. Copper coil was fed from a spool into the aluminum rig, which was rotated slowly (around 1 rotation per second) by a milling machine. A hand was placed on the copper wire spool in order to keep tension on the wire.

Two coils were affixed inside each rotor, as shown in Figure 4-5. Loctite 352, an epoxy which solidifies when exposed to ultraviolet light, was used as an adhesive. It was applied liberally to the coils, which were then set, and the rotor was then placed in an ultraviolet oven for 4 to 8 hours until the epoxy cured.

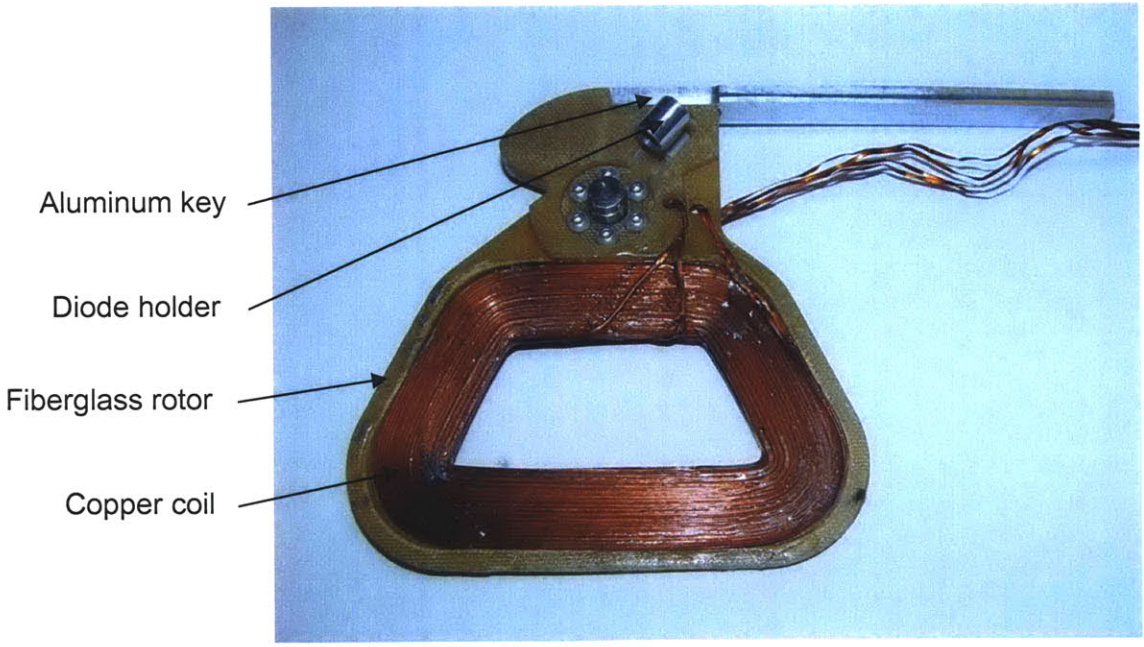

Figure 4-5. Two copper coils were affixed inside each fiberglass rotor.

4.2.1.1 Maximum current through coils

The maximum current, i_{max}, that can be passed through wire without causing the temperature of the wire, T_{wire}, to exceed the melting temperature of the bond coating (220 °C), is a function of the resistance of the wire R_{wire}, the area of the wire exposed to the air A_s, the ambient temperature T_{amb}, and the heat convection coefficitient h. The power, P, into the coil is

$$P = i^2 \cdot R . \tag{4.6}$$

At steady-state, this is equal to the heat dissipated by the coil, q'', which can be calculated using Newton's law of cooling

$$q'' = h \cdot A_s \cdot (T_{wire} - T_{amb}), \tag{4.7}$$

where A_s is the surface area of the wire exposed to the air, which is approximated at 0.00225 m^2 for each coil. By taking into account the thermal properties of air and the geometric set-up of the wire, the heat convection coefficient can be calculated to be approximately equal to 70 W/Km^2. Equating Equation 4.6 with Equation 4.7 and solving for i gives

$$i = \frac{\sqrt{h \cdot A_s \cdot (T_{wire} - T_{amb})}}{R_{wire}} . \tag{4.8}$$

The numerical value for i, or the maximum current that can be passed through the coil so that the coil temperature does not exceed 200 °C, is about 4 A. Since there are two wires per coil, twice as much current, up to 8 A, can be passed through the coil without exceeding the melting temperature. Peak currents can be up to three times this threshold, which is up to 24 A.

4.2.1.2 Calculated Natural Frequency

The expected natural frequency was calculated by modeling the rotor system as a linear second-order damped oscillator where I is the moment of inertia of the rotor, B is the damping parameter, K is the spring parameter, F is the external force acting on the rotor and θ is the angle of the rotor:

$$I \cdot \frac{d^2\theta}{dt^2} + B \cdot \frac{d\theta}{dt} + K\theta = F . \tag{4.9}$$

The natural frequency of the rotor, ω_n, is then:

$$\omega_n = \frac{K}{I} . \tag{4.10}$$

The spring parameter, K, is equal to the gravitational restoring force acting on the rotor:

$$K = mgd , \tag{4.11}$$

where m is the mass of the rotor, g is the gravitational force, and d is the distance between the rotational center of the rotor and the center of mass of the rotor as shown in . To simplify the calculation, the rotor was modeled as a disc with a radius of 60 mm. Using the parallel axis theorem, the moment of inertia of the disc model is:

$$I = \frac{1}{2} \cdot m \cdot r^2 + m \cdot d^2 , \tag{4.12}$$

where r is the radius of the disc, 60 mm, and d is the distance between the rotational center and the center of mass, 15 mm (see Figure 4-6).

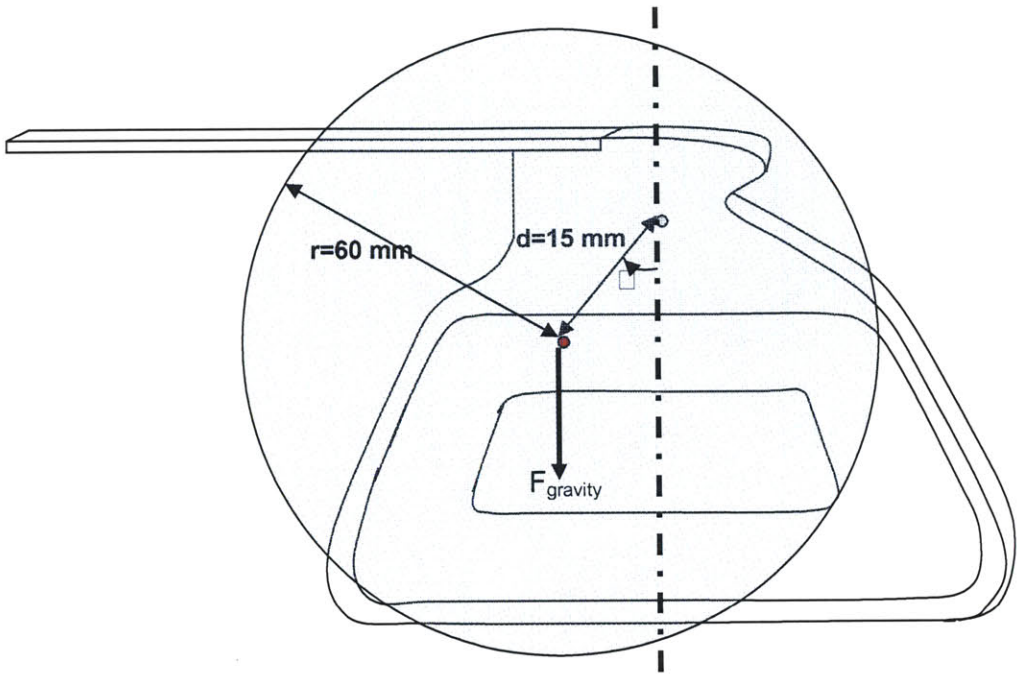

Figure 4-6. Model of rotor with shaded circle of radius 60 mm represented simplified rotor, the distance between the center of mass (red point) and the center of rotation 15 mm, and the gravitational force acting on the center of mass.

Combining Equations 5.10, 5.11 and 5.12 gives:

$$\omega_n = \frac{mgd}{\frac{1}{2}\cdot m\cdot r^2 + m\cdot d^2} = \frac{gd}{\frac{1}{2}\cdot r^2 + d^2} \tag{4.13}$$

Using $g = 9.8$ m/s^2, the resulting natural frequency is 8.6 rad/sec or 1.4 Hz. One way to increase the natural frequency is to move the center of gravity, thus changing d. Maximizing the natural frequency by changing d results in a $\omega_n = 10.85$ rad/sec or 1.73 Hz. As seen from Equation 4.13, the natural frequency is independent of the mass of the rotor.

4.2.2 Magnet Housing

Each rotor was surrounded by four custom-cut neodymium rare earth magnets (K & D Magnets, Inc.), two on each side, to create two separate magnetic fields going in opposite

directions. The magnets were encased in an aluminum housing designed and built by Dr. Eiji Hayashi (see Figure 4-7). The housing was designed such that the rotors could rotate more than 60 degrees and remain within the magnetic fields. Since the magnets were very strong, assembly of the housing required care. A rig was used to hold the magnet housing walls in line while being assembled. Stainless steel socket cap screws (M6 x 60) were screwed into one of the magnet housing walls to separate the two pieces. By unscrewing the screws, the top wall was slowly lowered towards the bottom wall (see Figure 4-8).

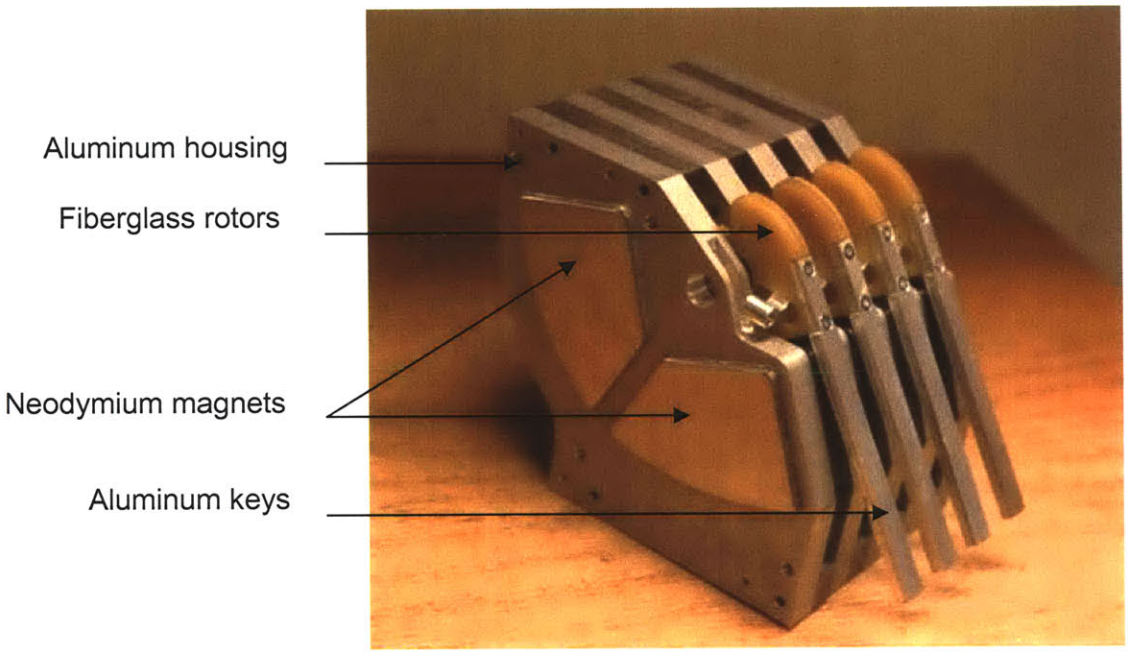

Figure 4-7. Four assembled actuators without electronic components.

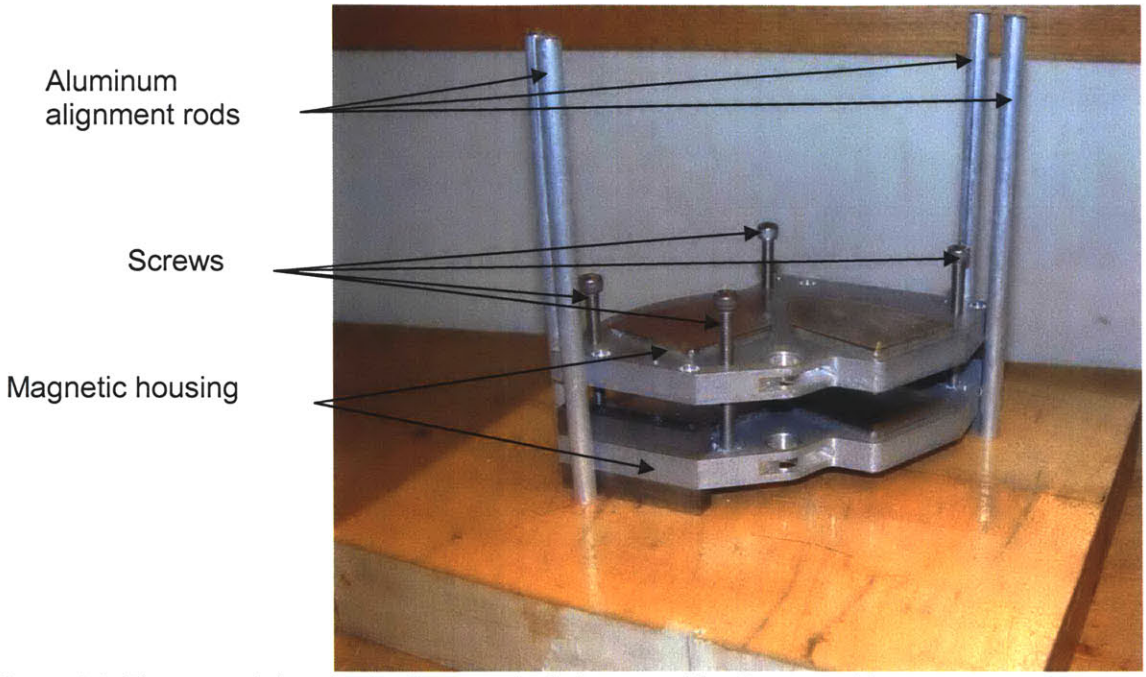

Figure 4-8. The magnetic housing in alignment rig during assembly. Because of the strong magnets, screws were used to gently lower one wall onto the other.

The magnetic housing walls contained fixtures for the ball bearings and rotor axles. During assembly, the rotor, ball bearings and washers were fixed into the walls. After the magnet housing walls were brought together, a rubber mallet was used to adjust the alignment of the walls such that the rotor could move freely, without scraping the walls. The walls were then secured into place with stainless steel screws.

4.3 Force Calibration

Two types of force sensors were used to calibrate the actuator. A Shimpo force gauge (Model FGV-0.5X–100X) was used to determine whether the current-force relationship of the actuators was linear. The force gauge was used on a single actuator using the set-up shown in Figure 4-9. As shown in Figure 4-10, the current-force relationship is linear, although the relationship depends on the angle of the rotor. As the angle decreases, the slope of the line also decreases, that is, more current is required for the same amount of force. This probably reflects the strength of the magnetic field that acts on the coil that

vary slightly depending on the angular position of the coil, due to the shape and position of the magnets. When the rotor rests at zero degrees, a bigger portion of the coil sits in the magnetic fields than when the rotor rests at -30 degrees.

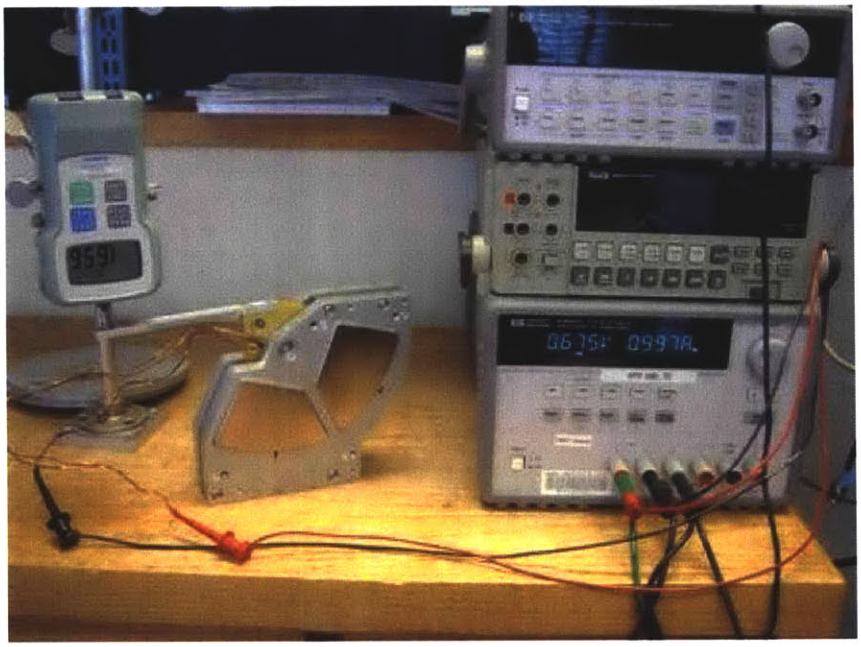

Figure 4-9. Set-up for initial force calibration on a single actuator.

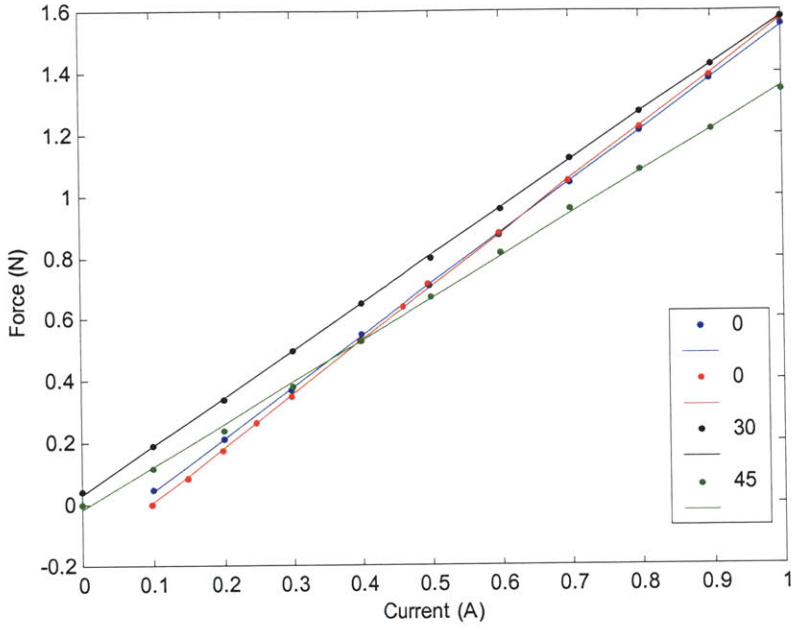

Figure 4-10. Force output as a function of current into rotor. Four different trials were done, two at 0 degrees (shown in diagram), one at 30 and one at 45 degrees.

A Futek Subminiature Threaded Button (Model LLB210) force sensor was used to calibrate the torque-current relation for the remaining four actuators. One advantage of the Futek sensor is that it outputs an analog voltage signal which can be read by a NIDAQ board and recorded by LabView. An aluminum fixture, shown in Figure 4-11, was designed and machined to hold the force sensor. The Futek sensor was pre-calibrated.

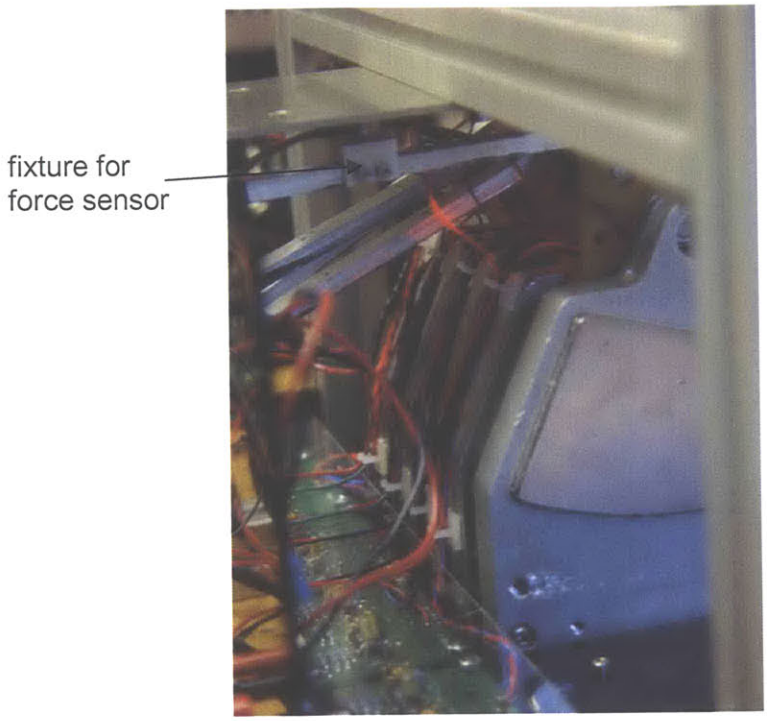

Figure 4-11. Side view of apparatus showing force sensor and aluminum fixture.

To calibrate the torque output of each rotor as a function of the input current, an aluminum plate was positioned over the Futek force sensor, which was held by the aluminum fixture, as shown in Figure 4-11. Between 0 and 2.5 A was then passed through the coils while the force from the actuator key was recorded. The relation between the current input and force output 75 mm from the rotational center for one rotor is shown in Figure 4-12. The resulting torque-current linear fits for each actuator are shown in Figure 4-13. As can be seen in the figure, each rotor has a slightly different torque-current relation. This is to be expected, since the coils in each rotor are not exactly identical. Rotors containing coils with more turns will have a greater slope (more torque for a given current) than those with fewer turns.

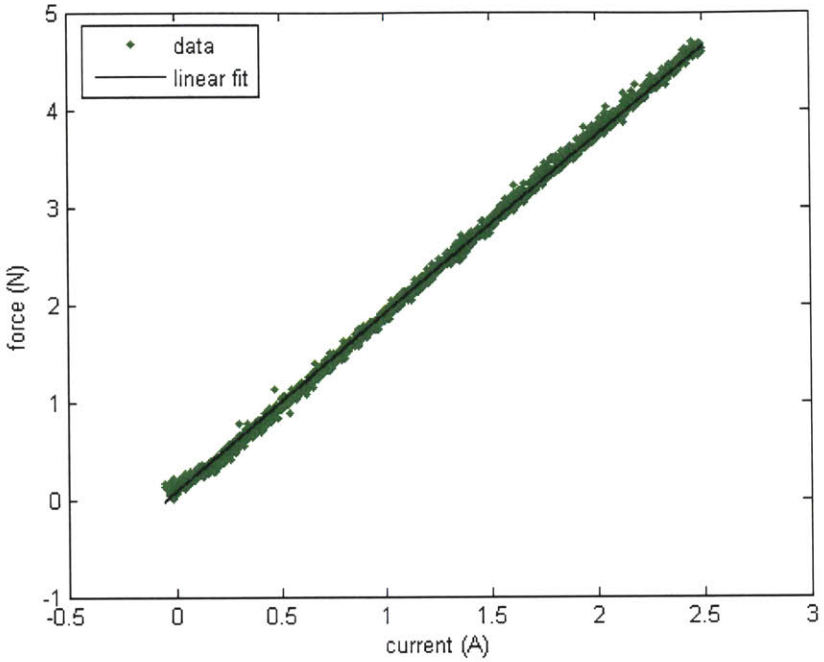

Figure 4-12. Force recorded vs. input current for Index rotor. The force sensor was placed 75 mm from the rotational center.

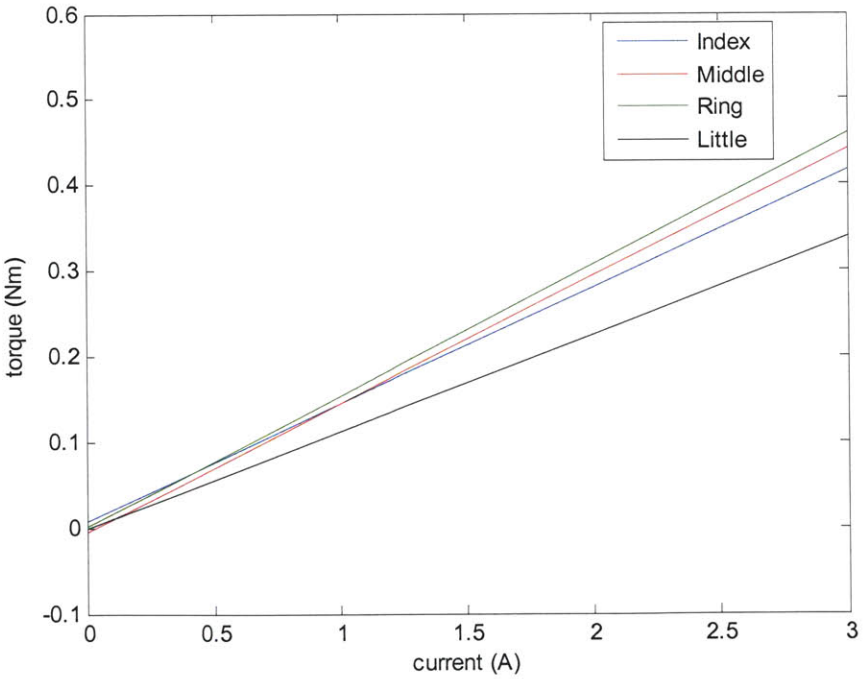

Figure 4-13. Torque v. current linear fits for all four actuators.

4.3.1 Maximum Torque and Force Output

The maximum continuous current that can be applied to the coils is 8 A. Using the force-current and torque-current calibration results above, the maximum continuous output torque and force for each actuator ranges from 0.91 Nm to 1.20 Nm and 12.1 N to 16.0 N, as listed in Table 2 . Peak torques and forces are three times these values, also listed in Table 2.

Table 2. Maximum continuous and peak forces and torques for actuators.

Actuator	Max Force (N)	Peak Force (N)	Max Torque (Nm)	Peak Torque (Nm)
Single	12.6	37.9	0.95	2.84
Index	14.5	43.5	1.09	3.27
Middle	15.3	45.9	1.15	3.45
Ring	16.0	48.0	1.20	3.60
Little	12.1	36.3	0.91	2.73

5 Characterization and Control of Actuator

In order to control the angular position and output force of the actuator, a control system was designed and implemented. The position of the actuator was measured using an optical system and the force was measured using a force gauge. An active controller was implemented using LabView. A control system was designed for a single actuator in a preliminary phase, then four control systems were designed for each of the four actuators, which had slightly different system characteristics from the first actuator. Each control system was designed to have a quick response time, zero steady-state error, and to remain stable with external disturbances.

5.1 Control Theory

Two different control systems were designed and implemented. To control the actuator's torque, open-loop control was used and to control the system's position, closed-loop feedback control was used.

5.1.1 Open-loop Control (Force control)

In the force controlled set-up, an input signal is passed through a controller and then to the actuator (see Figure 5-1). From Equation 4.4, the actuator's torque, and thus the force exerted on the finger, is proportional to the input current. Therefore, the force can be controlled directly by the input current.

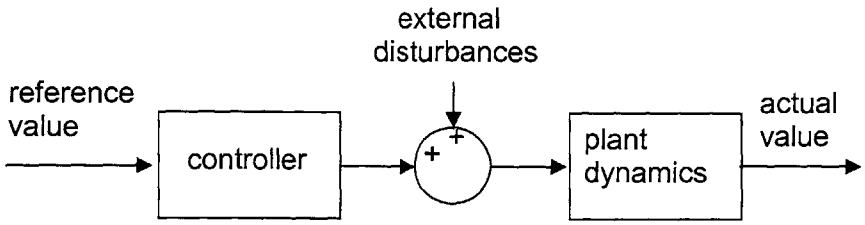

Figure 5-1. Simple open-loop control on plant.

The drawback of open-loop control systems is that they cannot compensate for external disturbances. This means that if additional external torques are exerted on the rotors, the current is not adjusted so that the net forces on the fingertips remain the same. To ensure that the forces exerted on the fingertips are the desired values, the control loop can be closed; that is, a force sensor can be used to measure the actual force which is then compared to the desired force. Although the force could have been more accurately controlled using closed-loop control, we chose open-loop control, since it eliminated the need for an additional force sensor.

5.1.2 Closed-loop Control (Position control)

A closed-loop control system consists of several elements: an input command or reference, a controller, and various sensors to measure the states of the system (see Figure 5-2). For our system, the controlled parameter was the angular position of the rotor. In the closed-loop control system, the measured angular position was compared to the desired, or reference, angular position and the difference, or the error, was sent through the controller and then to the actuator.

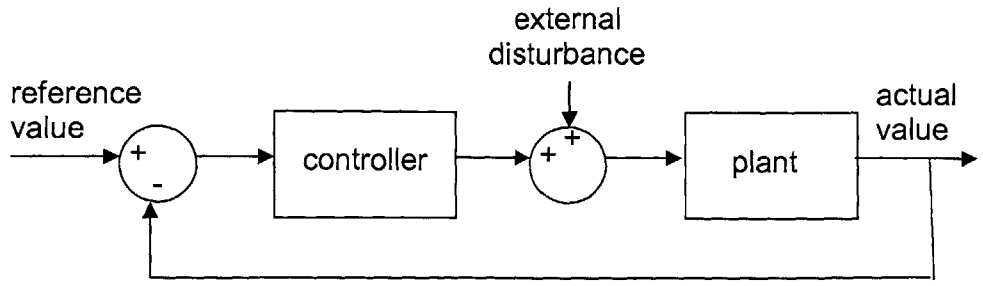

Figure 5-2. Simple closed-loop control system on a plant.

5.1.3 Proportional-Integral-Derivative Compensators

A proportional-integral-derivative (PID) compensator is used for the closed-loop controller. PID compensators are ideal and require active networks. A computer-controlled PID compensator was used rather than an op-amp circuit because its implementation was easier and more flexible: gain values for the elements in the computer-controlled compensator could be modified by changing an input to the computer as opposed to changing electronic components, such as resistors or capacitors, in an op-amp circuit.

When designing a PID compensator, the goal is to optimize the reduction of two characteristics: steady-state error and transient response time. A PID compensator is the sum of three elements: a proportional element (K_P), an integral element ($K_I \cdot \int$), and a derivative element ($K_D \cdot \frac{d}{dt}$):

$$G_{PID} = K_P + K_I \cdot \int + K_D \cdot \frac{d}{dt}.$$

The ideal integral compensator component reduces the system's steady-state error and the ideal derivative compensator improves the system's transient response time. By

adjusting each element's gains, the overall system can be optimized to fit the requirements of the user.

5.1.4 Discrete-Time Limitations

A computer serves as the system's compensator. Because computer processes, such as converting signals from analog to digital and performing operations on the data, are not instantaneous, the computer must sample data at discrete times. Discrete-time control introduces additional constraints on the system and affects the overall system's stability. As the sampling frequency decreases, the system becomes more unstable.

In order to optimize the performance of a discrete-time compensator, several things can be done. First, the sampling frequency can be increased by reducing time-intensive processes. This includes minimizing the number of operations performed on the data, or arranging the operations in parallel. Second, the gains of the system can be adjusted. Finally, the dynamics of the actuator can be altered. All three of these methods were applied to reduce the instability of the compensated actuator system.

5.2 Elements of Control System

The open-loop compensated system included a computer, which outputs the signal for the current, the amplifier, and the actuator (see Figure 5-3). For the open-loop system, the angular position was measured but not used to control the actuator.

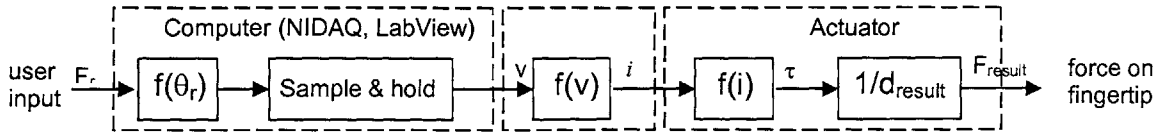

Figure 5-3. Open loop control for force controlled actuator.

The closed-loop compensated system included an angular position sensor, a computer, which received and output data through a National Instruments Digital-to-Analog Board and performed calculations for the compensator with LabView software, a power amplifier which converted a voltage signal output from the computer to a current, and the actuator, which translated a current input into a force and angle. The block diagram for the system is shown in Figure 5-4.

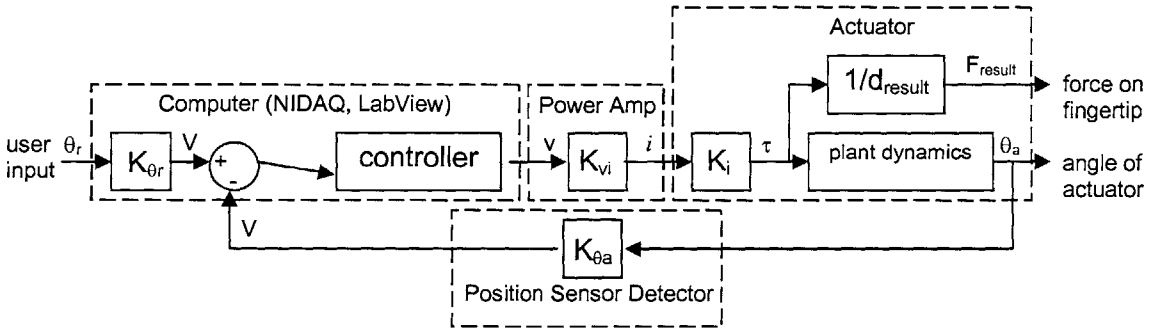

Figure 5-4. Block diagram of PID controlled actuator.

5.2.1 Position sensor

An optical system was used to measure the angle of the rotor. Although many other methods exist for measuring angular position, including Hall-effect sensors and potentiometers, an optical system was implemented because of its accuracy and its lack of interference with the system dynamics. The optical system consisted of laser diodes, which emit light at a specified frequency, a linear position sensor detector, and a signal processing circuit.

Laser diodes were used to emit light, in preference to light emitting diodes (LEDs), because they require less power and do not heat up as fast. The laser diodes (Sanyo DL3147-021, Thorlabs) had an output wavelength of 645 nm and required 5 mW of power. Each diode was placed in a 5.6 mm diameter cylindrical aluminum housing

affixed to each rotor. In order to reduce the likelihood of saturating the diode with voltage during a power surge, a 68.1 Ω resistor was placed in series with each laser diode. A single constant-current power supply (Hewlett Packard) was used to power all four diodes, which were arranged in a parallel circuit. Screwed in the end of each aluminum housing was a 5.6 mm diameter glass aspheric lenses (Thorlabs, Inc) to collimate the laser beam. When the rotor rotates, the laser beam changes its orientation. A one-dimensional position sensor detector, or PSD (S3932, Hamamatsu), mounted on the magnet housing, detected the location at which the beam struck it. The S3932 model has an active area of 1 mm by 12 mm.

The PSD was connected to a PSD signal processing circuit (C3683-01, Hamamatsu). A single constant current power supply (Hewlett Packard) was used to power all four circuits. The position signal was fed into a NIDAQ board and sampled by LabView. The voltage output of each circuit varied linearly with the position at which the laser beam struck the PSD.

5.2.1.1 Position Calibration

The position sensor detection system was initially calibrated to determine if the voltage output from the PSD was a linear function of the angular position. To do this, a ruler was set up vertically at the tip of the key of the assembled actuator. During the calibration measurements, the voltage from the PSD was sampled by a NIDAQ board (PCI-6052E and PCI-MIO-16XE-10) and recorded by LabView. The key was then displaced and held for several seconds at a particular location on the ruler (see Figure 5-5). This procedure was repeated for twenty different positions.

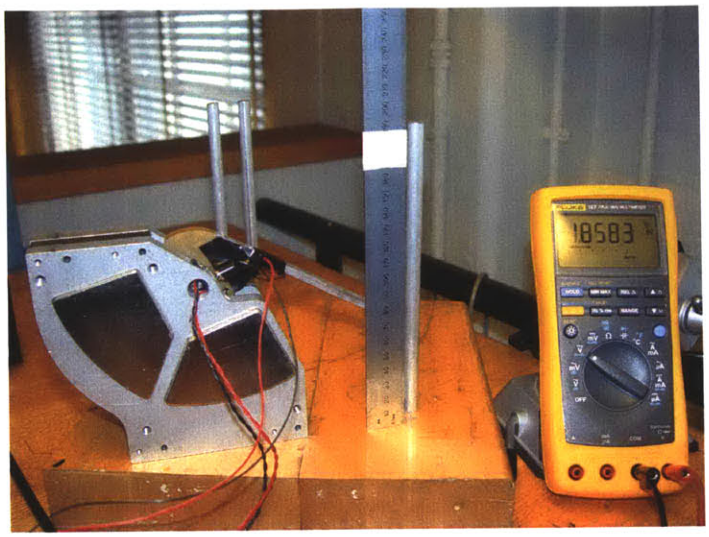

Figure 5-5. Set-up for initial calibration.

The corresponding angle of the rotor was calculated from the readings on the ruler (see Figure 5-6). The relationship relating the angle with the position on the ruler is:

$$\theta = \tan^{-1}\left(\frac{D + \frac{m}{\cos\theta} - d}{w}\right),$$

where D is the height of the center of rotation, m is the distance between the center of rotation and the key, d is the height of the tip of the key (measured with the ruler), and w is the horizontal distance between the center of rotation and the ruler. Matlab was used to calculate the angular position.

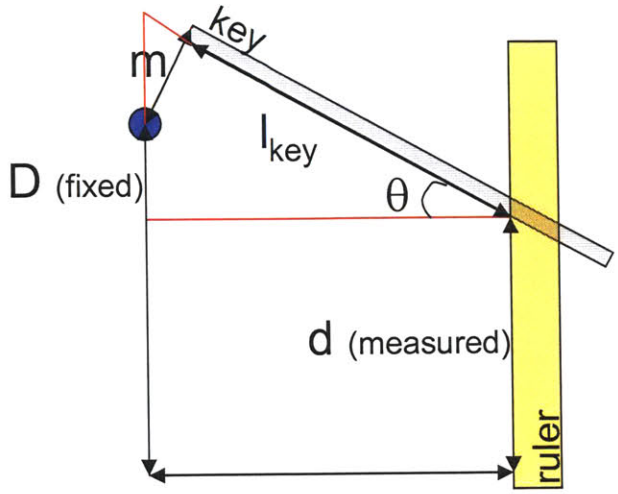

Figure 5-6. Geometry of the set-up for calibration.

The average voltage reading for each position was then plotted against the calculated angle of the position, as shown in Figure 5-7. As can be seen in the figure, the output voltage is not a strictly linear function of the rotor angle, as it deviates at the extreme positions of the key (above 0 degrees, below 50 degrees). This is probably due to the nonlinear path that the diode travels during rotation. However, since the margin of error is within 1%, over the range of key excursion (0 to 60 degrees), the voltage-angle relationship can be approximated as a linear function.

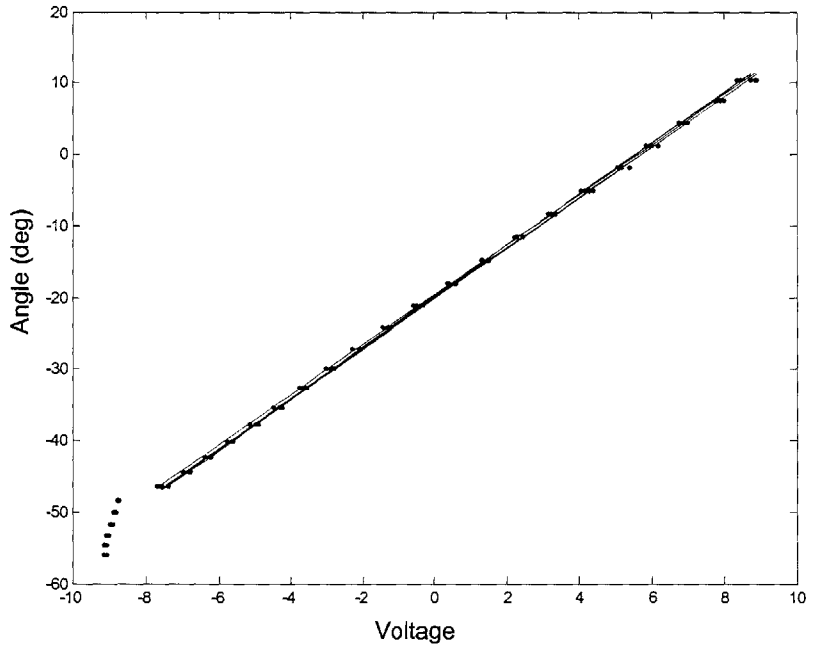

Figure 5-7. Angle of rotor as a function of the voltage output. The blue points are the raw data, the lines are the linear fits for three trial runs.

The laser diodes are very sensitive to disturbances, such as current spikes, changes in ambient light, or movement and therefore the intensity of the output light can vary each time they are turned on. The variation in light intensity results in a change in the angle-voltage curve. Because of this sensitivity to external disturbances, the position

sensor system was calibrated before each experiment. All four actuator rotors were calibrated at once using a Labview program and Matlab script (see Appendix B).

5.2.2 Computer System (Labview, NIDAQ)

Two NIDAQ boards (PCI-6052E, PCI-MIO-16XE-10), each with 2 output and 16 input channels, were used to sample data and control the inputs to the actuators. LabView was used to communicate with the NIDAQ boards and as the compensator. The sampling frequency was limited by the computer. The fastest sampling frequency that could be used was 125 Hz. To avoid aliasing, the fastest frequency that could be measured for the actuator was half this, 62.5 Hz.

5.2.3 Power Amplifier

Four Techron 8501 power amplifiers were used to convert the voltage signal from the D/As to a current. The amplifier's gain could be adjusted manually. A 3 A fuse was placed in series between each amplifier and actuator, in case the system became unstable and currents higher than 3 A were delivered to the actuators. A schematic of the system set-up is shown in Figure 5-8.

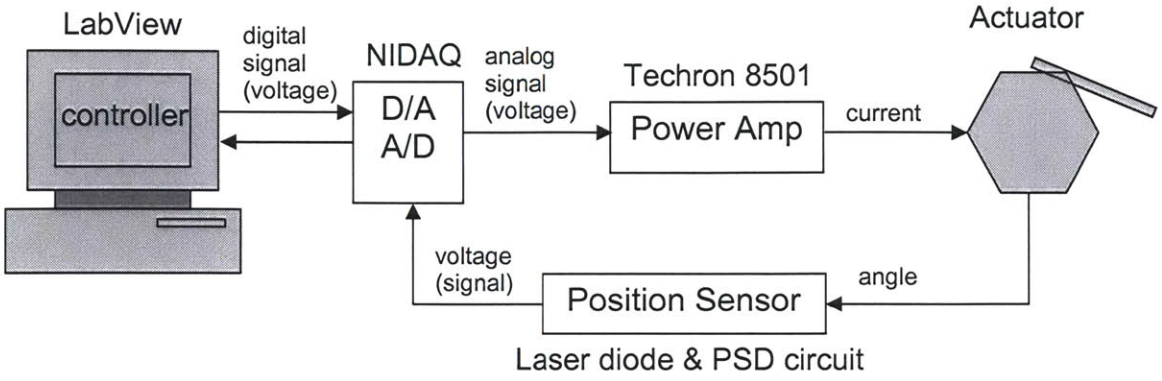

Figure 5-8. Schematic of set-up of controlled actuator.

5.3 Characterization (step response, frequency response)

Before a compensator could be designed, system characterizations had to be completed. For each actuator, the time and frequency responses were calculated. For the step response, a square wave input current, which ranged from -50 mA to +50 mA, was delivered to each actuator. For the single actuator, a natural response was found by releasing the actuator from a horizontal position and allowing it to oscillate freely. For the frequency response of each actuator, a Labview program was designed that created sine waves, ranging in frequency from 1 Hz to 100 Hz, and recorded the response of each actuator. A Matlab program was then created that analyzed the data and plotted the frequency response.

5.3.1 Single Actuator

A single actuator was characterized and controlled before the multi finger apparatus was built. This actuator was slightly different from the actuators in the apparatus in that it did not have extra wires attached to the key, resulting in lower damping and a slightly lower inertia (see Figure 5-9). The natural response and frequency response of the single actuator are shown in Figure 5-10 and Figure 5-11, respectively. The natural response is fit with a second order model with natural frequency, ω_n= 11.7 rad/sec and damping ratio, ζ=0.10. The natural frequency is close to the natural frequency calculated in Section 4.2.1.2 of 8.6 rad/sec.

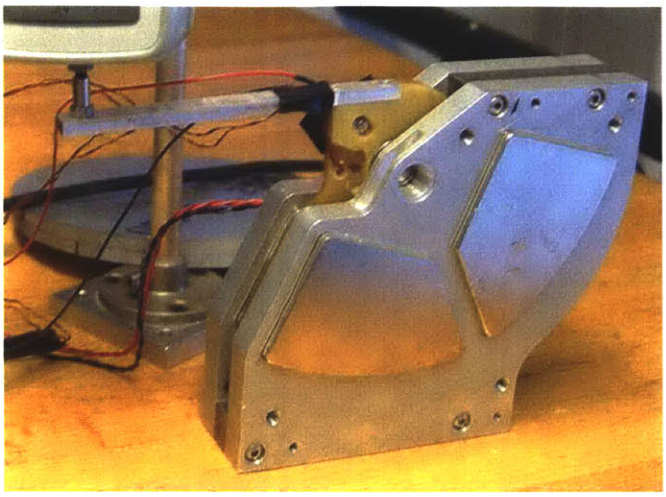

Figure 5-9. Single actuator set-up.

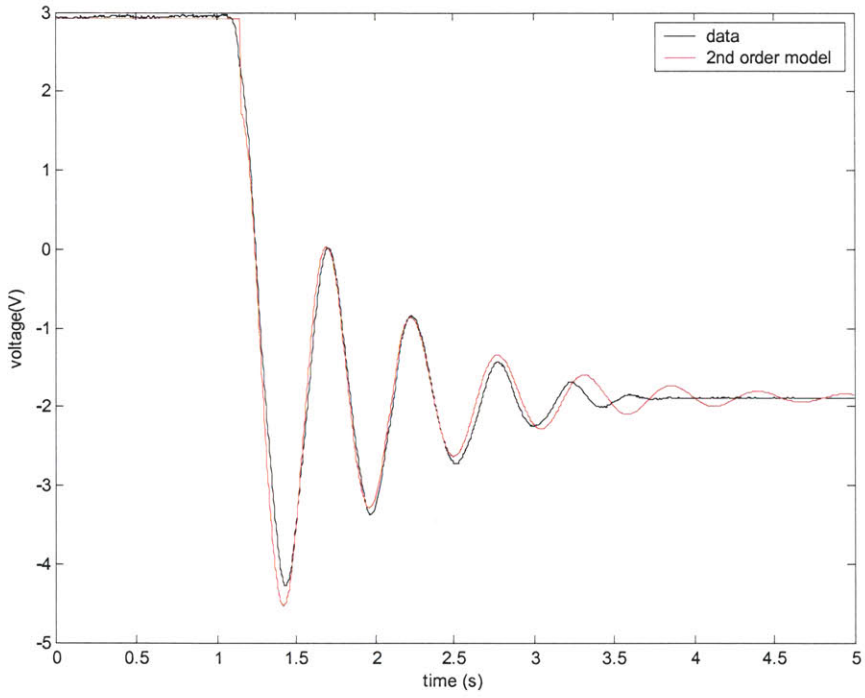

Figure 5-10. Natural response of single actuator released from 0 degrees fit with 2nd order model with ω_n=11.7 and ζ=0.10.

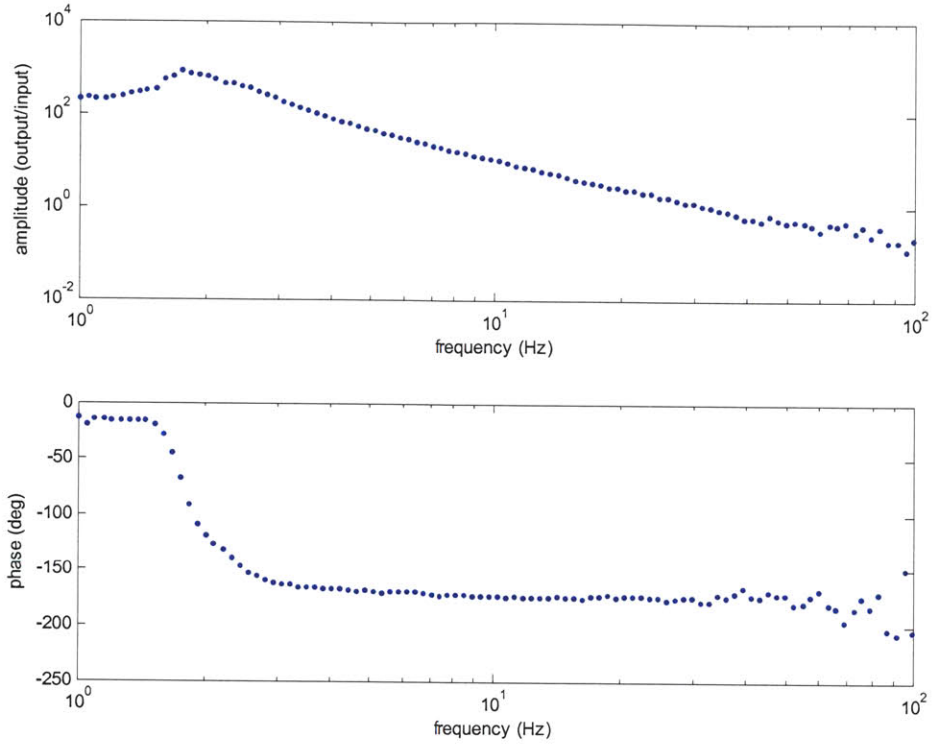

Figure 5-11. Frequency response of single actuator.

5.3.2 Four Actuators for Multi finger apparatus

The step response of each actuator in the multi-finger apparatus is shown in Figure 5-12. The frequency responses are shown in Figure 5-13. As can be seen in the figures, each actuator has a slightly different characterization because of different external forces, including damping from the attached wires. It can also be seen that all actuators were non-linear; that is, the step response varied depending on the angle of the actuator. Although the actuators were non-linear, their responses are repeatable, as shown in Appendix C. The index and middle finger actuators are more damped than the ring and little finger actuators. This can also be seen in the frequency responses of the actuators, as shown in Figure 5-13, in which the amplitude of the ring and little finger actuators is

greater at their resonance frequencies. The middle finger actuator demonstrated the most bizarre behavior: the magnitude of oscillation at its resonant frequency was two orders of magnitude lower than the other three actuators at about 10 dB as opposed to about 40 dB. Although there could be several reasons for this, the most likely reason is that the rotor rubbed slightly against the magnet when it rotated which increased the friction of the rotor which leads to an increase in damping. This problem can be fixed by either widening the space between the magnet housing, by introducing spacers, or by realigning the rotors so that they rotate more parallel to the housing walls.

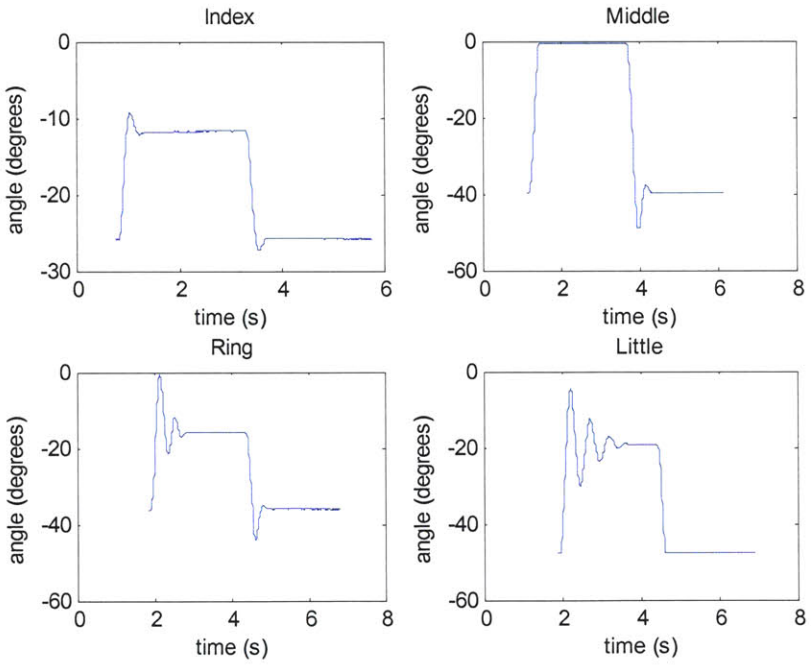

Figure 5-12. Step response for four actuators. All actuators were given a square wave input -50 mV to +50 mV.

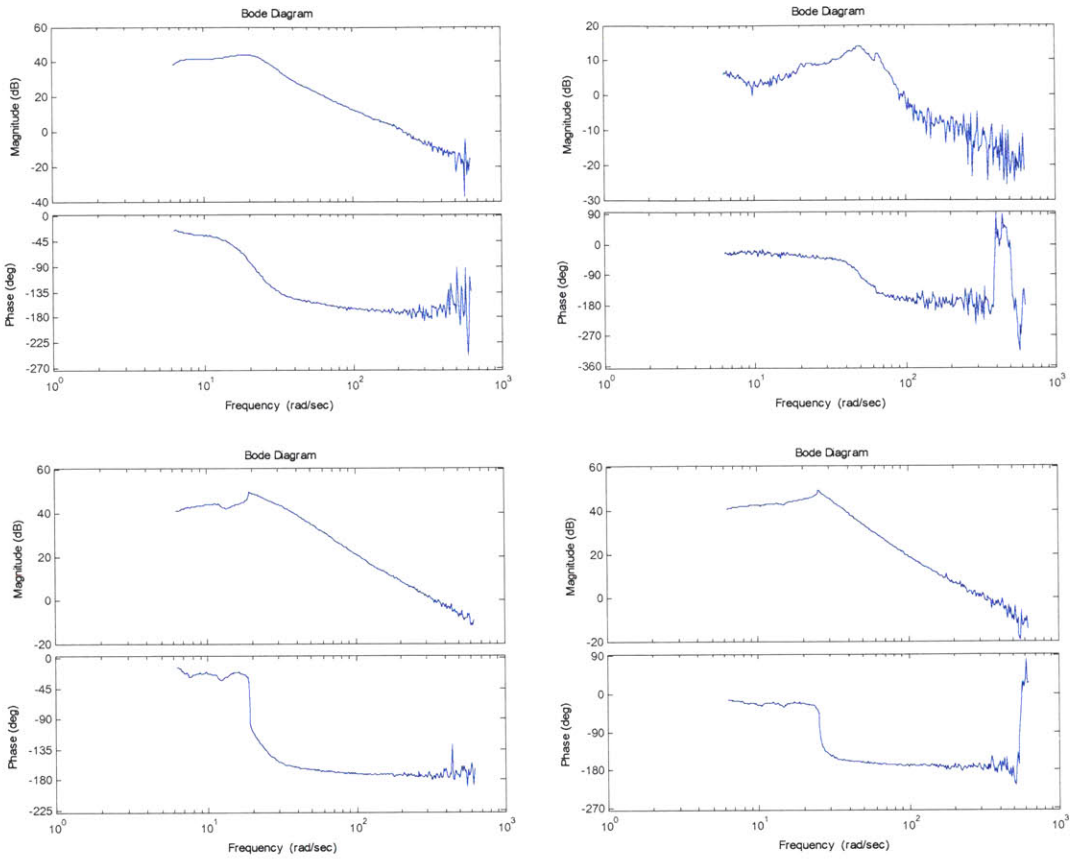

Figure 5-13. Frequency responses for the four actuators. From top left and going clockwise: Index, middle, little and ring finger actuators.

5.4 Compensator Design

Each actuator had a different characterization and so separate PID compensators were designed for each.

5.4.1 Single Actuator

For the single actuator, the Propotional Gain Response had a steady-state response time of about 3 s and a large steady-state error (See Figure 5-14). By introducing an integral element in the control system, the steady-state error was eliminated but the response time was not significantly improved. Introducing a derivative element improved the response

time but did not eliminate the steady-state error. The PID response (in the lower right) had a steady state error of zero and a steady-state response time of less than 1 second.

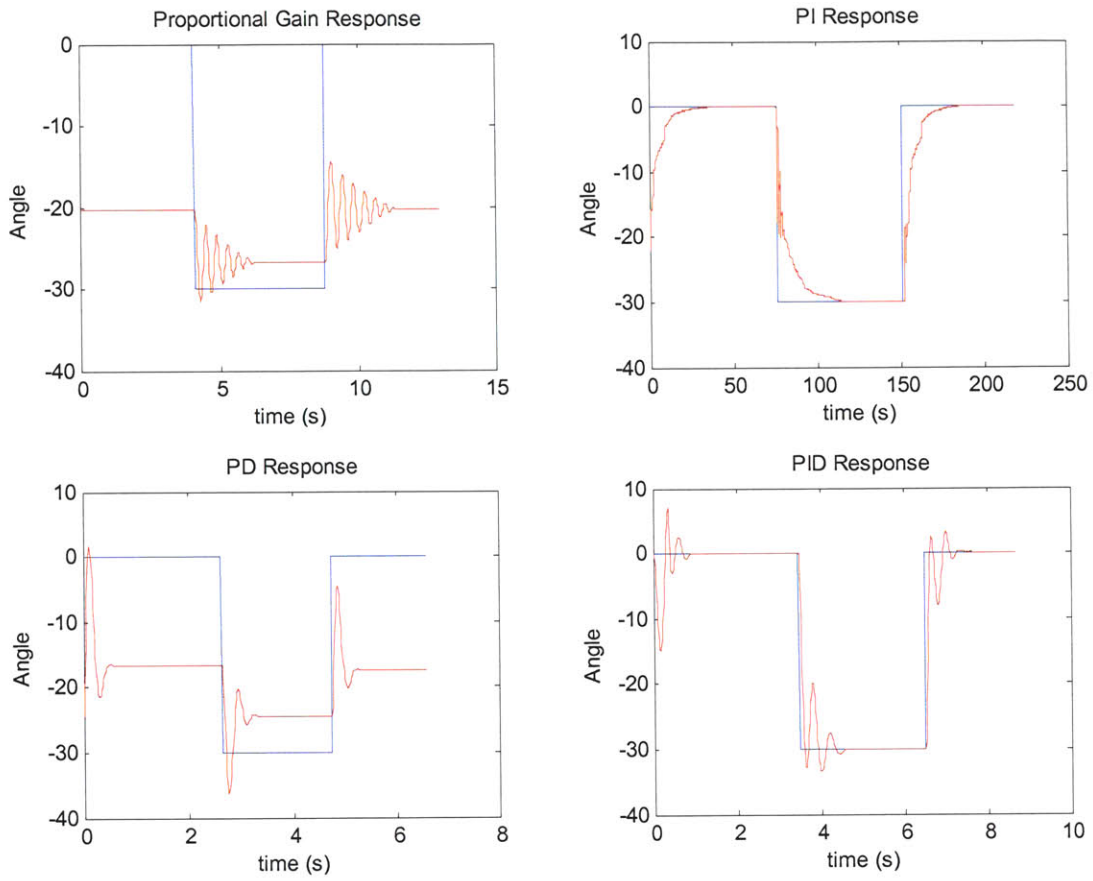

Figure 5-14. Step response of actuators with P,PI,PD,and PID controllers.

5.4.2 Four Actuators for Multi finger apparatus

As previously mentioned, each actuator had a different step and frequency response, so it was necessary to customize a control system for each actuator. The resulting Proportional Gain, Proportional-plus-Integral, Proportional-plus-Derivative, and Proportional-plus-Integral-plus-Derivative responses for each actuator are shown in Figure 5-15, Figure 5-16, Figure 5-17, and Figure 5-18. The percent overshoot, steady-state settling time, and steady-state error are summarized in Table 3.

As can be seen in all four responses, the steady-state error improved greatly with the compensated system. However, this improvement sometimes resulted in a slower response time, as was the case for the index and ring finger actuators. The response time for the middle finger actuator did not improve with the controlled system, staying at 0.6 seconds, but the steady-state error reduced to zero.

Further modifications of the control system can lead to faster response times with no steady-state error. Changing the gains of the feedback loop, allowing more than 3 A of current to pass through each rotor, or introducing a more intelligent feedback loop that can change the gains in the feedback system depending on the position or velocity of the actuator could be used to improve the rotor response.

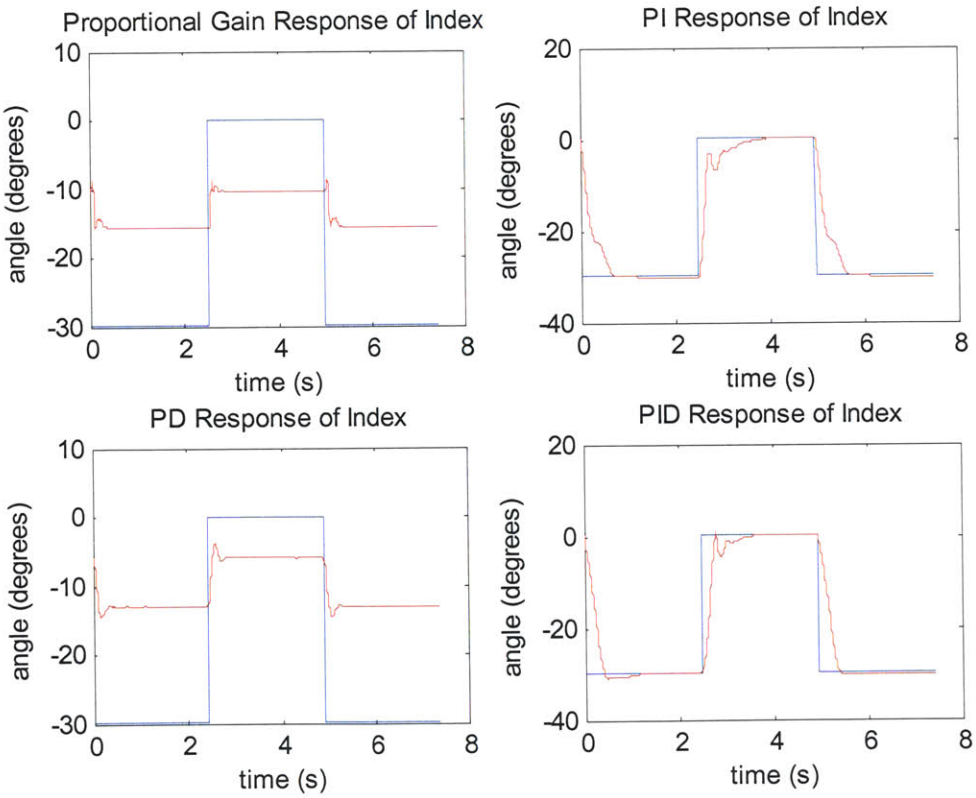

Figure 5-15. Controlled feedback response of the actuator for the index finger.

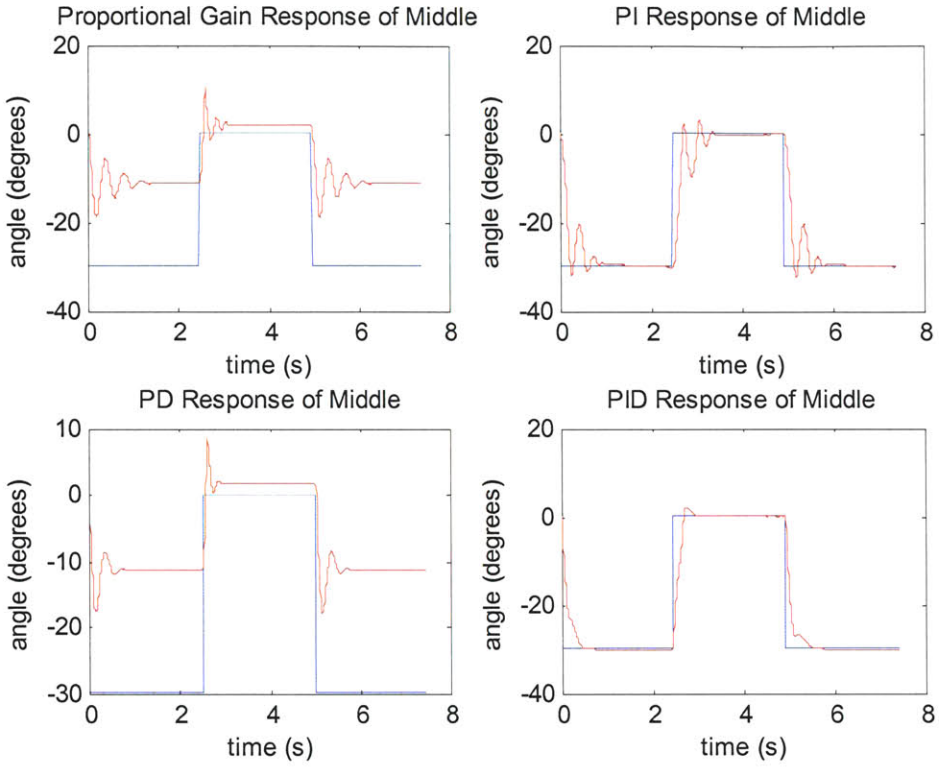

Figure 5-16. Controlled feedback response of the actuator for the middle finger.

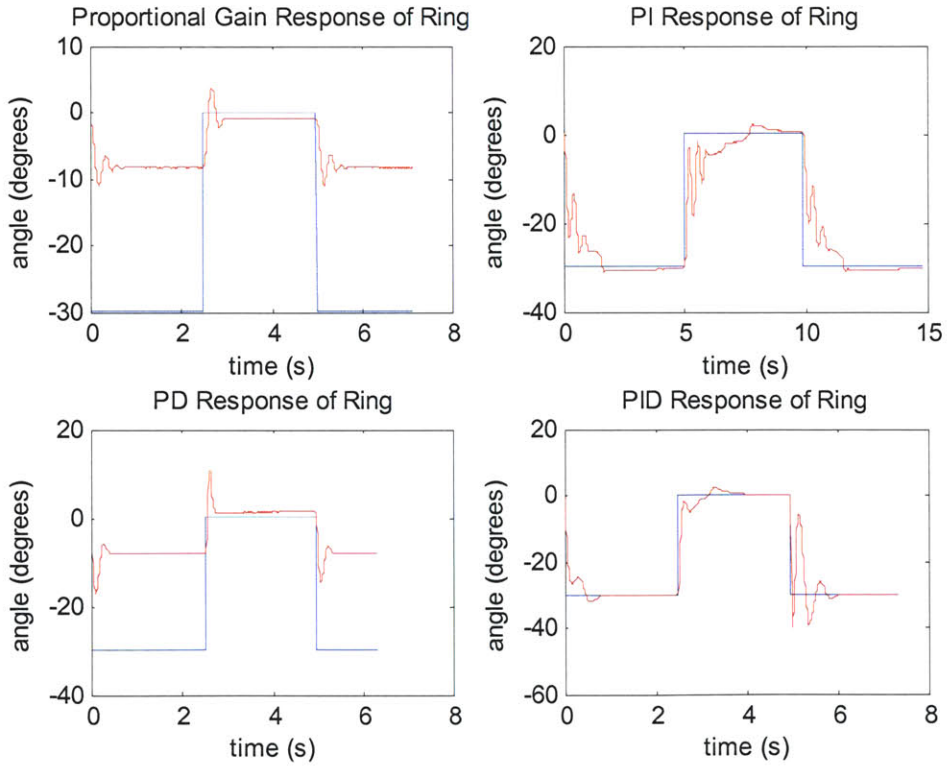

Figure 5-17. Controlled feedback response of the actuator for the ring finger.

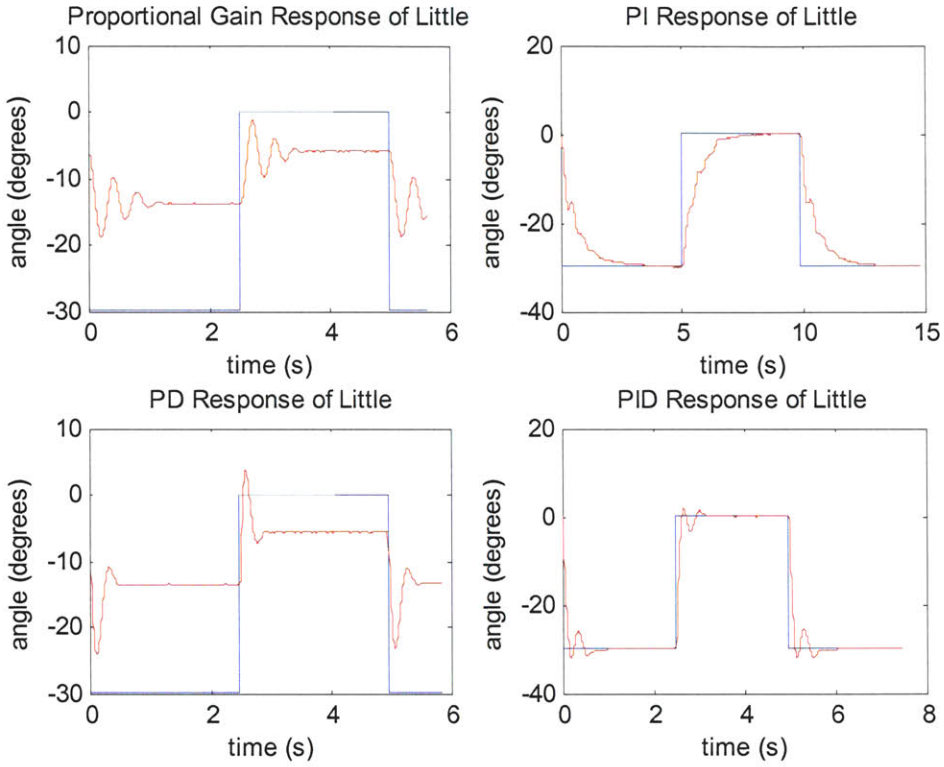

Figure 5-18. Controlled feedback response of the actuator for the little finger.

Table 3. Summary of characteristics of responses for all actuators: % OS, time to reach steady-state, and steady-state error.

Actuator	Uncontrolled: % OS	Uncontrolled: Steady-state time	Uncontrolled: Steady-state error	Controlled: %OS	Controlled: Steady-state time	Controlled: steady-state error
Single	71%	~2 s	Up to 20°	28%	0.8 s	0
Index	20%	0.5 s	11°	3.5%	1.3 s	0
Middle	23%	0.6 s	10°	7.6%	0.6 s	0
Ring	80%	0.9 s	19°	7.7%	1.5 s	0
Little	56%	1.8 s	20°	5.9%	0.8 s	0

6 System and Human Interface

Several features were added to the apparatus in order for it to be used for human testing. Keys and finger holders were constructed to provide a place for the fingers to rest and a platform was constructed for the wrist to rest. Finally, a surrounding box was constructed to protect the apparatus.

6.1 Keys

Aluminum keys were designed and machined by Dr. Hayashi. The keys were mounted on the rotors to provide a place for the fingers to rest.

6.1.1 Finger Holders

In order to hold the fingers on the keys of the actuators while the rotors moved, finger holders were made. The finger holders were designed to fit snuggly around each of four fingers while translating forces exerted on the fingers from the rotor keys.

Since the rotational axis of the rotor is not at the same point as the rotational axis of the MCP joint, the contact point between the finger pad and rotor key needed to move as the angle of the rotor changed. A holder was needed that would easily move while the key rotated. A holder that slid along the length of the key was chosen because it was a simple design that did not require additional linkages.

The finger holder was made of three parts: a finger splint (DeRoyal), a Velcro strap (DeRoyal), and a Teflon slider. The finger splint was oriented such that the splint opening allowed the finger pad to contact the key. The splint opening was widened so that the entire finger pad could make contact with the key. The Velcro strap was threaded through two slits at the base of the splint so that it could be wrapped around and

secured above the PIP joint of the finger. The slider was machined from Teflon which slides easily along aluminum. One surface of the Teflon was treated with Chemigrip Cement (Saint-Gobain Performance Plastics Corp), an etching solution, before it was bonded to the finger holders. A specialized epoxy, BONDiT B-45TH (McMaster-Carr) was used to adhere the Teflon slider to the splints. Figure 6-1 shows the finger holder assembly. A total of 11 finger holders with a range of sizes were made in order to accommodate testing subjects with different sized fingers.

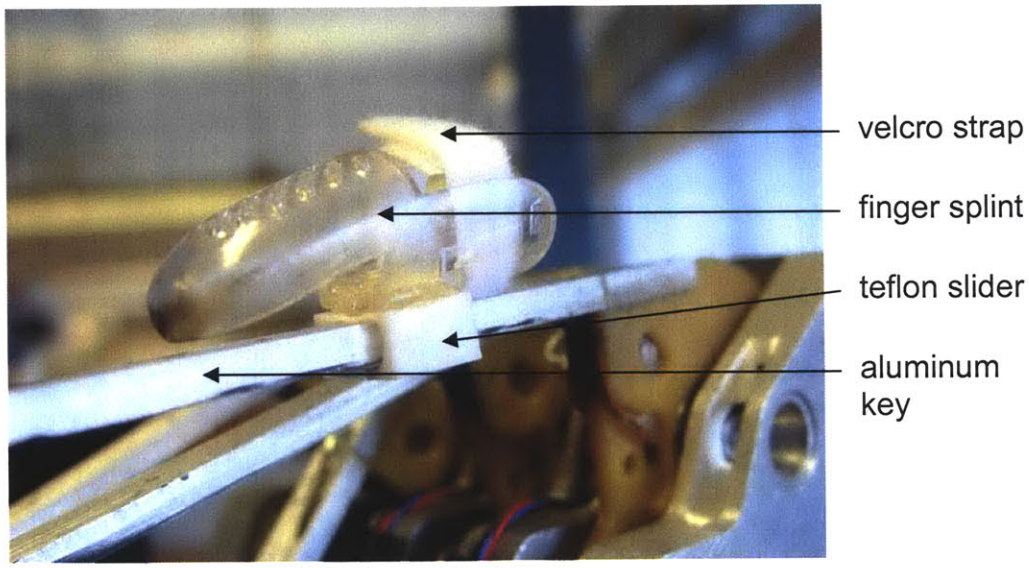

Figure 6-1. One finger holder resting on a key. The finger holder consisted of a finger splint glued to a Teflon slider. A Velcro strap secures the holder to the finger.

6.1.2 Attachment wires

Since rotation of the rotor included movement of the embedded coil, it was necessary to arrange the wires so that they could move easily with the rotor but not interfere with the keys' movement. The wire also needed to be attached in a way that would not lead to breakage with repetitive motion.

Machined into each aluminum key was a canal 5 mm wide and 3 mm deep. The copper coil from the rotor was then run along the length of the wire. Stranded, insulated, electrical wire (20 AWG) was soldered onto the end of the copper magnet wire.

The attachment of the electrical wire added additional dynamics to the system. It increased the damping of the keys slightly and occasionally, wires would cause the keys to "stick" into one position. The wires were carefully arranged to minimize interference with other keys and to prevent sticking (see Figure 6-2).

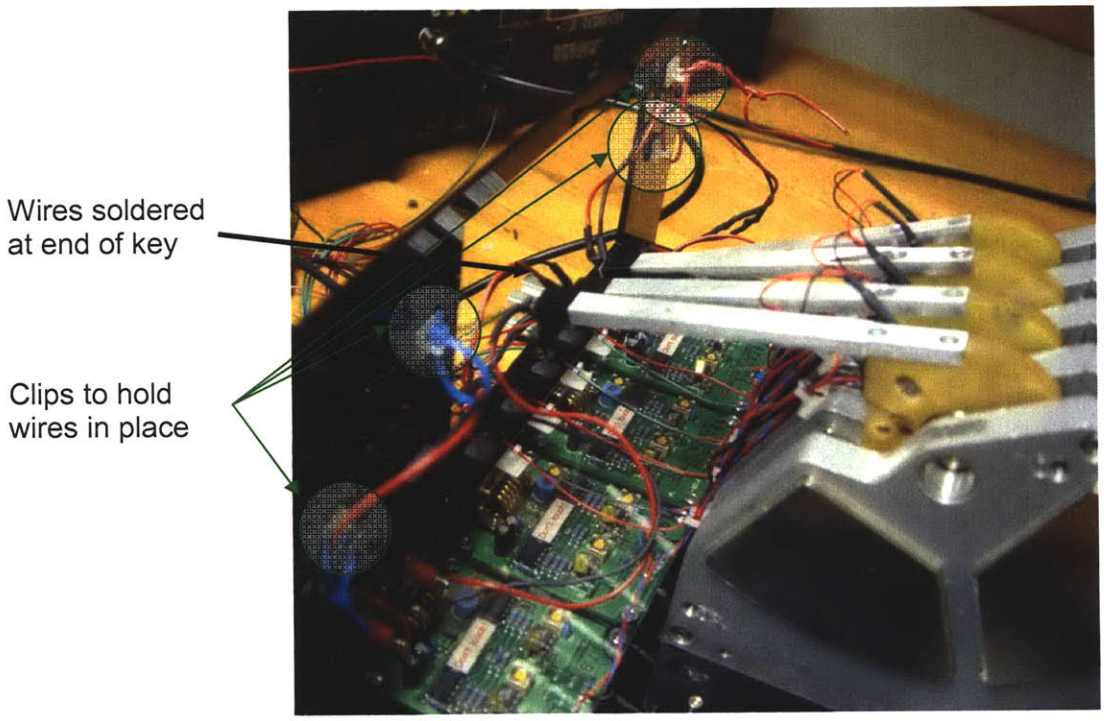

Figure 6-2. Wires are arranged to interfere as little as possible with movement of key.

6.2 Wrist Rest

A platform was made in order to provide a place for the wrist to rest during experiments. It was constructed using MK Systems Profile Technology (MK Automation, Inc) and covered with felt. The wrist rest can be adjusted up and down and side-to-side to accommodate different sized arms and hands (see Figure 6-3).

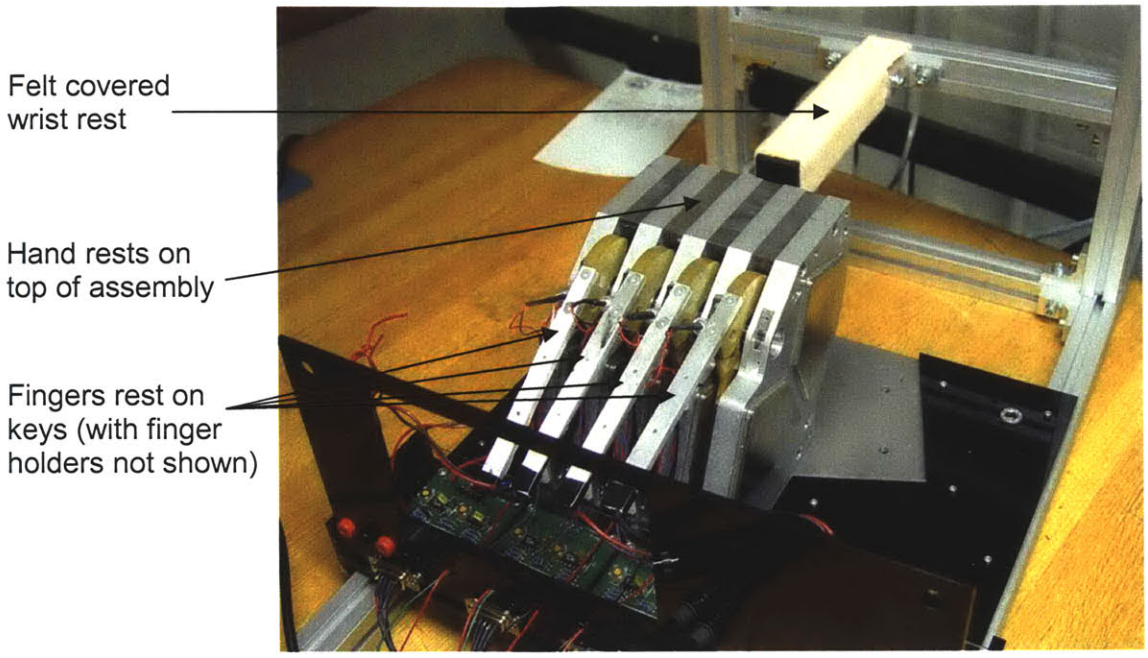

Figure 6-3. Interior of actuator box cover, showing the felt-covered wrist rest.

6.3 Surrounding Box & electronic interface

A surrounding box was constructed from MK Systems Profile Technology with black acrylic panels (see Figure 6-4). It served several purposes. It protected the apparatus from magnetic materials and dust. The box also darkened the interior which made the position sensor system more consistent and easier to implement. Finally, an electronic interface was constructed that was included in the surrounding box. The electronic interface provided an accessible way to power the actuators and communicate with the sensors on the actuator.

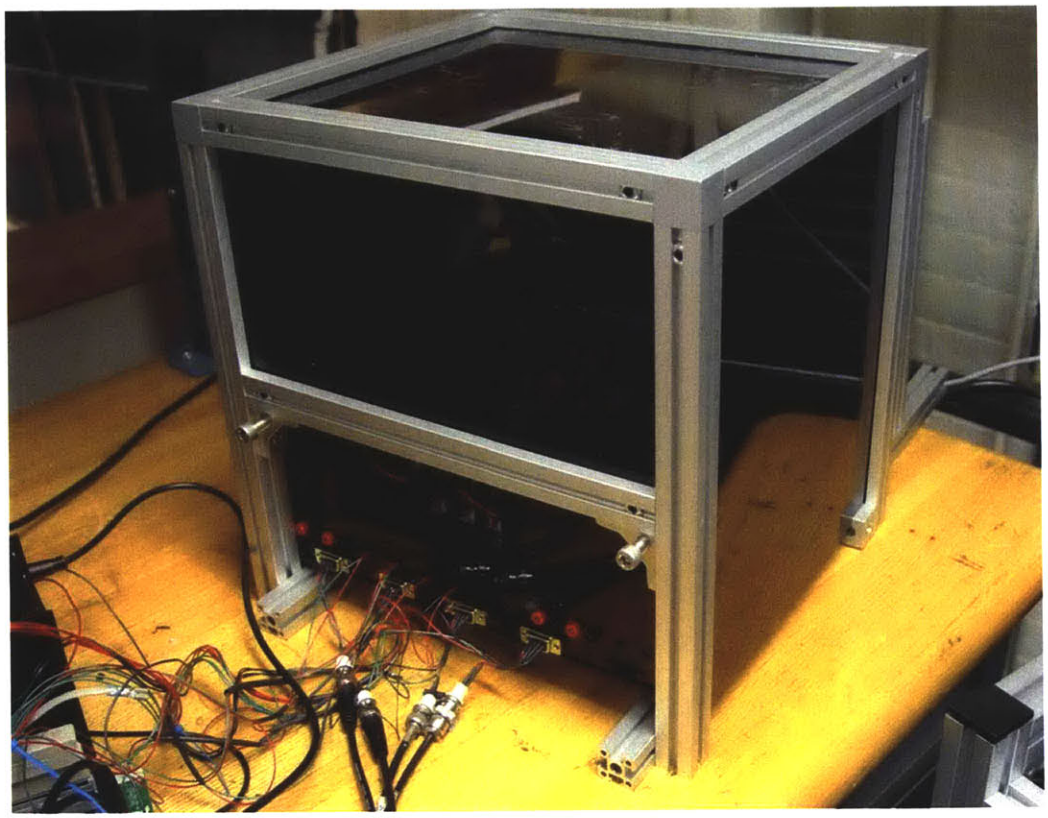

Figure 6-4. The surrounding box of the actuator assembly.

6.4 Human Interface

The completed design allowed experimental subjects to place their hand on the top of the actuator assembly and secure his fingers in the finger holders that slid along the length of the keys. The box was able to enclose the arm and hand comfortably. Figure 6-5 shows a hand in the intended orientation on the actuator assembly. The surrounding box was removed for demonstration purposes.

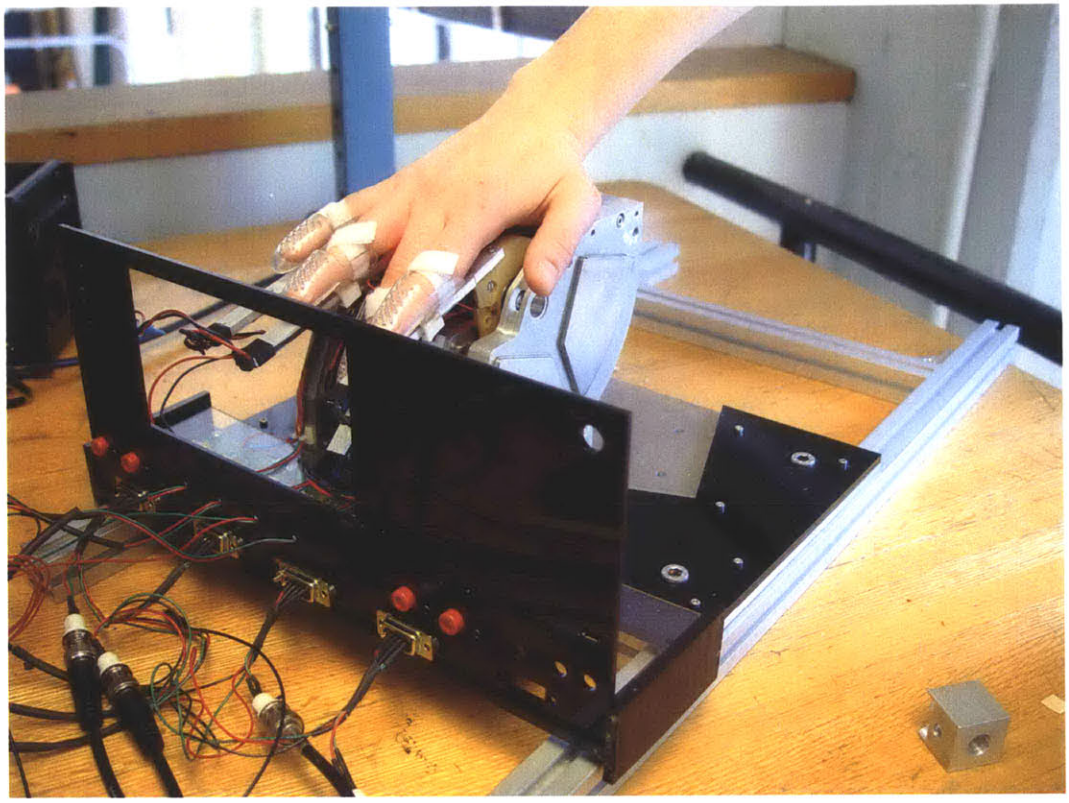

Figure 6-5. Hand with finger holders on actuator assembly (surrounding box left out in for demonstration purposes).

7 Conclusion

In this thesis, the design and construction of a position-controlled, multi finger haptic display that uses electromechanical voice-coil actuators is described. The purpose of the display is to perform studies of the human hand. The force exerted by the actuators can be controlled with an open-loop system. The actuators can also be position controlled with a closed-loop feedback system. Additional structures provide an interface for test subjects.

7.1 Design Improvements

Several changes could be made with the current apparatus or a second generation device that would improve the steady-state response of the actuators. Copper coil, which has a density of 8920 kg/m^3 was used for the rotor coils. Replacing the copper coil with aluminum, which has a density of 2700 kg/m^3, would result in a rotor with a lower weight. Although a lower weight would not change the natural frequency of the rotor, as shown in Equation 4.13 in Section 4.2.1.2, it would result in a rotor with a lower inertia. Rotors with lower inertia require less torque, and thus less energy, to move. A rotor with aluminum embedded coils would respond quicker to a given command, and would be easier to control.

One advantage copper has over aluminum, however, is that it has a higher thermal and electrical conductivity; that is, the thermal and electrical resistance of copper is higher than aluminum. This allows us to pass more current through a copper coil than an aluminum coil without the copper coil overheating. Although aluminum coils will result in a more responsive system, copper coils allow for a more powerful system.

Another improvement to the existing design would be to increase the distance between the magnets in the housing. In the current design, the distance between the magnets is 5 mm and the width of the rotor is 3 mm. The reason for placing the magnets close together is to increase the intensity of the magnetic field between them and to keep the width of the actuators low (23 mm for the current design). However, although the clearance allows for 1 mm of clearance on each side of the rotor, any misalignment will result in the rotor rubbing against the magnets. This results in additional friction which causes a reduction in the response time and controllability of the actuators. Although increasing the distance between the magnets would result in a lower intensity magnetic field, it would reduce the occurrence of rotor rubbing and improve actuator response.

An additional way to reduce the damping of the actuators is to find an alternative arrangement for the wires that, in the current design, are affixed to the end of the actuator keys. The wires were affixed to the end of the keys in order to provide a place for the users' fingers to interact with the device without interfering with the wiring and to reduce the likelihood that the wires would break. However, the wires add additional damping to the rotors and sometimes cause the rotors to "stick." An alternative arrangement in which the wires would interact less with the dynamics of the rotors but not interfere with the user and not break off easily would result in a better design.

Finally, the control system for the actuators would have less overshoot and a faster response time with a faster sampling rate. The present rate of 125 Hz limits the frequency which can be measured to half this, 62.5 Hz. A faster sampling rate would lead to a faster response rate, less overshoot and a lower steady-state response time. A

faster computer processor would allow the control system to have a faster sampling rate, and thus an improved response.

7.2 Future Directions

The apparatus developed is capable of both force-control and position-control, it is possible to use the device for many different types of hand studies. One possible experiment would be to test the biomechanical and neural contribution to finger coupling. In this experiment, subjects would place their hands on the device and be told to move a finger at a comfortable pace. The position of each key would be recorded to see how individual target finger movement affected the movement of other fingers, similar to the experiment conducted by Hager-Ross and Schieber (2000). Afterwards, the recorded position of the target key would be played back while the positions of the other keys would be recorded. Unlike the Hager-Ross and Schieber study, this experiment would allow a direct comparison of the movement of the non-target fingers during active and passive movement of the target finger. Any additional movement during active motion of the target finger could then be attributed to neural constraints. Similarly, any reduction in movement during the active motion of the target finger could be attributed to the effects of active movement control.

Other experiments that require force feedback or position control, or both, can also be performed using the actuator assembly. In conclusion, the multi-finger apparatus should permit a number of experimental studies of human hand function to be undertaken in which the contribution of individual fingers to force and position control can be quantified and modeled.

References

Becker, J. D., and C. D. Mote, 1990, "Identification of a Frequency Response Model of Joint Rotation," *Journal of Biomechanical Engineering*, Vol 112, pp. 1-8.

Burdea, G. C., 1996, *Force and Touch Feedback for Virtual Reality.* New York: John Wiley & Sons, Inc.

Burdea, G., J. Zhuang, E. Roskos, D. Silver, and N. Langrana, 1992, "A Portable Dextrous Master with Force Feedback," *Presence: Teleoperators and Virtual Environments*, Vol. 1, pp. 18-28.

Burdea, G. C., and P. Coiffet, 2003, *Virtual Reality Technology*. Hoboken, NJ: Wiley-Interscience, pp. 41-53, 92-109, 234-231.

Bureau of Labor Statistics: http://www.bls.gov/

Dennerlein, J. T., E. Diao, C. D. Mote, Jr., and D. M. Remple, 1999, "*In Vivo* Finger Flexor Tendon Force while Tapping on a Keyswitch," *Journal of Orthopaedic Research,* Vol 17, pp. 178-184.

Gerard, M. J., T. J. Armstrong, J. A. Foulke, B. J. Martin, 1996, "Effects of Key Stiffness on Force and the Development of Fatigue While Typing," *American Industrial Hygiene Association Journal*, Vol. 57, pp. 849-854.

Gillespie, B., 1994 "The Virtual Piano Action: Design and Implementation," Proceedings of the International Computer Music Conference, Aahus, Denmark, Sept 12-17, 1994. pp. 167-170.

Gillespie, B. and M. Cutkosky, 1992, "Dynamical Modeling of the Grand Piano Action," Proceedings of the International Computer Music Conference, San Jose, CA Oct 14-18, 1992, pp. 77-80

Gomez, D., G. Burdea, and N. Langrana, "The Second Generation Rutgers Master – RM II," *Proceedings of Automation '94 Conference, Taipei, Taiwan,* Vol. 5 pp. 7-10.

Gordon, A. M., A. Casabona, and J. F. Soechting, 1994, "The learning of novel finger movement sequences," *Journal of Neurophysiology,* Vol. 72, pp. 1596-1610.

Hager-Ross, C., and M. H. Schieber, 2000, "Quantifying the Independence of Human Finger Movements: Comparisons of Digits, Hands, and Movement Frequencies," *The Journal of Neuroscience*, Vol. 20 (22), pp. 8542-8550.

Hajian, A. Z., and R. D. Howe, 1997, "Indentification of the Mechanical Impedance at the Human Finger Tip," *Journal of Biomechanical Engineering*, Vol. 119, pp. 109-114.

Hayashi, E., M. Yamane, and H. Mori, 1994, "Development of a Moving Coil Actuator for an Automatic Piano," *International Journal of Japan Society of Precision Engineering,* Vol. 28 No. 2, pp. 164-169.

Hayashi, E., M. Yamane, and H. Mori, 1999, "Behavior of piano-action in a grand piano for an automatic piano," *Pioneering International Symposium on MOVIC in Mechantronics*, Tokyo, April 6-7, 1999.

Immersion Corporation: http://www.immersion.com/

Ishii, M., and M. Sato, 1994, "A 3D Spatial Interface Device Using Tensed Strings," *Presence*, Vol 3, No 1, Winter 1994, pp. 81-86.

Jones, L., 1997, "Dextrous Hands:Human, Prosthetic, and Robotic,"*Presence*, Vol 6, No 1, February 1997, pp. 29-56.

Jones, L., and S. Lederman, In press. *Human Hand Function.* New York: Oxford University Press.

Kato, I., and K. Sadamoto, 1987, *Mechanical Hands Illustrated.* New York: Hemisphere Publishing Corporation, pp. 3-34.

Keen, D. A., and A. J. Fuglevand, 2003, "Role of intertendinous connections in distribution of force in the human extensor digitorum muscle," *Muscle & Nerve*, Vol. 28, pp. 614-622.

Kilbreath, S. L., R. B. Gorman, J. Raymond, and S. C. Gandevia, 2002, "Distribution of the forces produced by motor unit activity in the human flexor digitorum profundus," *Journal of Physiology,* 543.1, pp. 289-296.

Kunesch, E., F. Binkofski, and H.-J. Freund, 1989, "Invariant temporal characteristics of manipulative hand movements," *Experimental Brain Research,* Vol. 78, pp. 539-546.

Leuschke, R., E. K. T. Kurihara, J. Dosher, and B. Hannaford, 2005, "High Fidelity Multi Finger Haptic Display," *First Joint Eurohaptics Conference and Symposium on Haptic Interfaces for Virtual Environment and TeleOperator Systems* (WC '05), pp. 606-608.

Madden, J. D., N. Vandersteeg, P. G. Madden, A. Takshi, R. Zimet, P. A. Anquetil, S. R. Lafontaine, P. A. Wieringa, and I. W. Hunter, 2004, "Artificial Muscle Technology: Physical Principles and Naval Prospects," *IEEE Journal of Oceanic Engineering,* Vol. 29, No. 3, p. 706

Martin, B. J., T. J. Armstrong, J. A. Foulke, S. Natarajan, E. Klinenberg, E. Serina, and D. Rempel, 1996, "Keyboard Reaction Force and Finger Electromyograms during Computer Keyboard Work," *Human Factors*, Vol. 38 (4), pp. 654-664.

Mathiowetz, V., N. Kashman, G. Volland, K. Weber, M. Dowe, and S. Rogers, 1985, "Grip and Pinch Strength: Normative Data for Adults," *Archives of Physical Medicine and Rehabilitation,*, Vol 66, February 1985, pp. 69-74.

National Center for Health Statistics: http://www.cdc.gov/nchs/

National Institution of Occupational Safety and Health: http://www.cdc.gov/niosh/homepage.html

Ohki, Y., B. B. Edin, and R. S. Johansson, 2002, "Predictions Specify Reactive Control of Individual Digits in Manipulation," *The Journal of Neuroscience*, Vol 22 (20), pp. 600-610.

Ohtsuki, T., 1981, "Inhibition of Individual Fingers during Grip Strength Exertion," *Ergonomics,* Vol. 24, No. 1, pp. 21-36.

Radwin, R. G., and S. Oh, 1992, "External Finger Forces in Submaximal Five-finger Static Pinch Prehension," *Ergonomics*, Vol. 35, No. 3 pp. 275-288.

Reilly, K. T., and M. H. Schieber, 2003, "Incomplete Functional Subdivision of the Human Multitendoned Finger Muscle Flexor Digitorum Profundus: An Electromyographic Study," *Journal of Neurophysiology*, Vol. 90, pp. 2560-2570.

Salthouse, T. A., 1984, "Effects of Age and Skill in Typing,"*Journal of Experimental Psychology: General,* Vol. 113, No. 3, pp. 345-371.

Salthouse, T. A., 1986, "Perceptual, Cognitive, and Motoric Aspects of Transcription Typing," *Psychological Bulletin,* Vol. 99, No. 3, pp. 303-319.

Schieber, M. H., and M. Santello, 2004, "Hand function: peripheral and central constraints on performance," *Journal of Applied Physiology,* Vol. 96, pp. 2293-2300.

SensAble Technologies: http://www.sensable.com/

Shaffer, L. H., 1982, "Rhythm and Timing in Skill," *Psychological Review,* Vol. 89, No. 2, pp. 109-122.

Shimoga, K. B., 1992, "A Survey of Perceptual Feedback Issues in Dextrous Telemanipulation: Part I. Finger Force Feedback," *Proceedings IEEE Virtual Reality Annual International Symposium, VR '93, September 18-22, 1993, Seattle, Washington*, pp. 263-270.

Tan, H. Z., N. I. Durlach, C. M. Reed, and W. M. Rabinowitz, 1999, "Information Transmission with a Multifinger Tactual Display," *Perception & Psychophysics*, Vol. 61 (6), pp. 993-1008.

Tubiana, R., 1981, *The Hand.* Philadelphia: W. B. Saunders Company.

Westling G. and R. S. Johansson, 1987, "Responses in glabrous skin mechanoreceptors during precision grip in humans," *Experimental Brain Research,* Vol 66, No 1, pp. 128-140.

Zatsiorsky, V. M., Z. Li, M. L. Latash, 1998, "Coordinated force production in multi-finger tasks: finger interaction and neural network modeling," *Biological Cybernetics,* Vol. 79, pp. 139-150.

Appendix A: Resistance of Coils

The resistance of each coil made was measured by a mega ohm meter (Fluke 1520 MegOhmMeter). Since the clamps had a significant resistance, compared to the resistance of the coils, the were subtracted from the measured resistance to get the actual resistance. The 'resistance length' was then calculated. Notice that the resistance of the coils are fairly consistent, as shown in Table A-1. Also note that the resistance, and thus the 'resistance length,' of coil #4 is abnormally high. This could have been due to a faulty connection between the ohm meter clamps and the wire, or incomplete removal of the insulating polyamideimide coating on the wire.

Coil #	Resistance measured	Corrected resistance	'Resistance Length'
1	1.83	1.48	14.8
2	1.66	1.31	13.1
3	1.60	1.25	12.5
4	2.89	2.64	26.4
5	1.64	1.29	12.9
6	1.66	1.31	13.1
7	1.95	1.60	16.0
8	1.72	1.37	13.7
9	1.70	1.35	13.5
10	1.69	1.34	13.4
11	1.75	1.40	14.0
12	1.73	1.38	13.8
13	1.67	1.32	13.2
14	1.68	1.33	13.3
15	1.70	1.35	13.5

Table A- 1. Resistance of coils (corrected by subtracting resistance of ohmeter clamps). By multiplying resistance by 0.126 ohms/meter (the resistance of the wire), "resistance length" was calculated.

Several layers of each coil were removed before the coil was glued into the rotor. This changed the length, and thus the resistance, of each coil. Also, each rotor had two coils affixed on the inside, so that a given amount of current could produce twice as much

force. The resistance of each rotor was measured, which included the extra wires attached on the outside of the rotor. These resistances are listed in Table A-2.

Rotor	**Resistance (in ohms)**
Index	**1.10**
Middle	**1.12**
Ring	**1.21**
Little	**1.18**

Table A- 2. Resistance of each rotor, with two coils per rotor and additional wires attached externally.

Appendix B: Quick Position Sensor Calibration

Because the laser diodes were sensitive to disturbances, and the output light intensity varied with continued use, the actuator position sensors were calibrated before each experiment. All four actuators were calibrated at once by clipping them together. While recording the voltage output with LabView, the keys were held at zero degrees and then moved through their entire angular range of motion (see Figure B-1). A Matlab program was written to calculate the fitted linear relation between the voltage output and angular position for each actuator rotor (see Figure B-2).

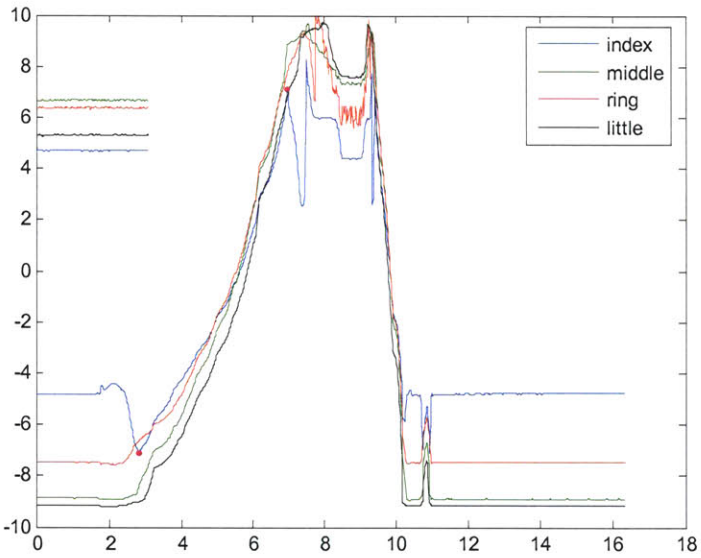

Figure B-1. Output voltage of PSD while moving actuators through entire range of motion (straight lines between 0 and 2 is voltage of actuators held at zero degrees). Raw data is processed by a Matlab program that calculates linear relation for angle and voltage.

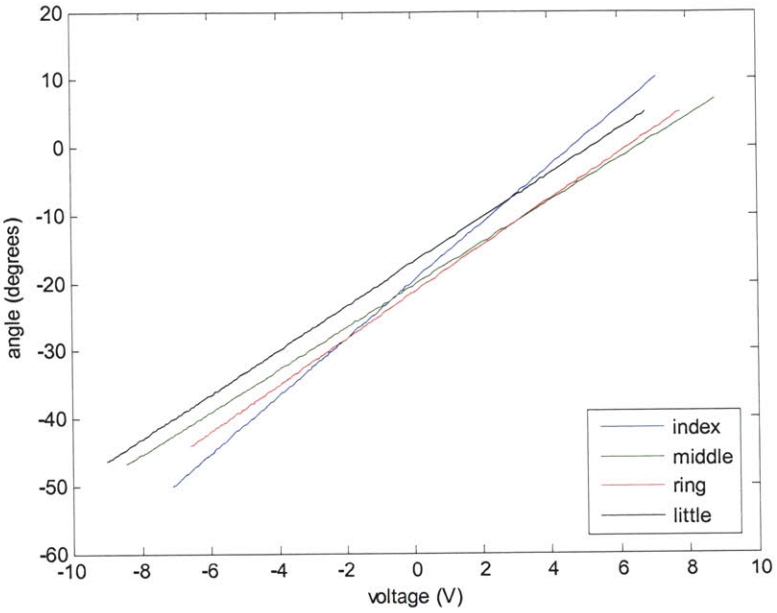

Figure B-2. Linear fits of angle vs. Voltage for all four actuators.

Appendix C: Repeatability of Actuator Step Responses

Although each actuator had different step responses, and the characteristic time response depended on the angle of the actuator (that is, it was non-linear), each actuator did show repeatability in their responses. Shown in Figure C-1 is each actuator responding to a current step input over several cycles. Note that the y axis is voltage output from the position sensitive detector and not the angle of the actuator.

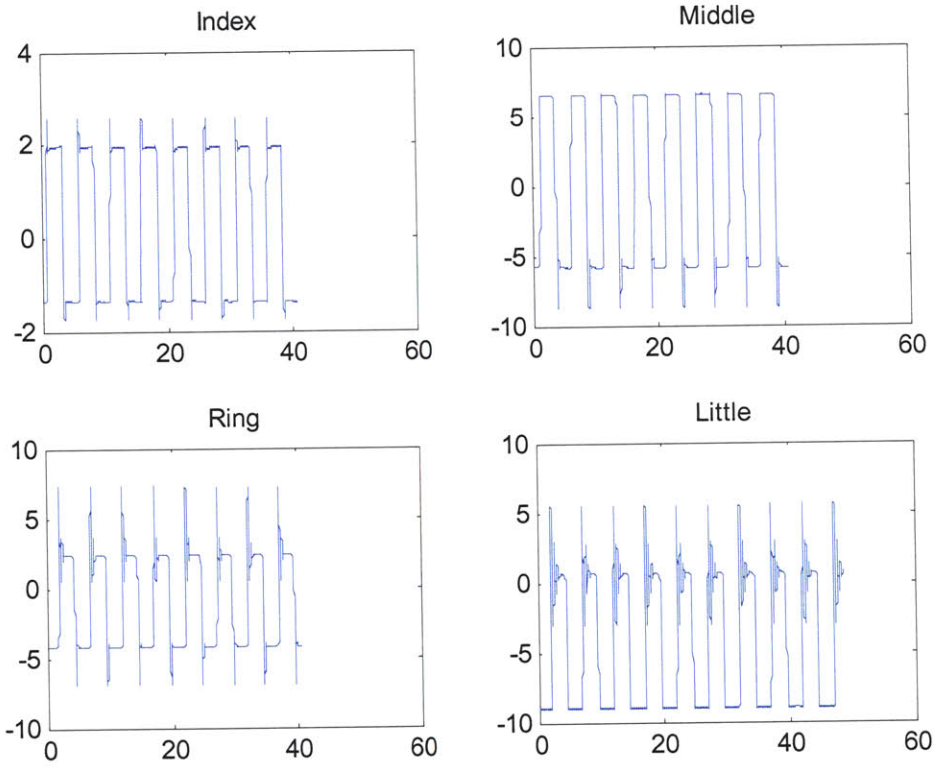

Figure C-1. All four actuators responding to several current step inputs. The y axis is voltage output from the position sensitive detector, and not angle of the actuator.

Appendix D: LabView GUI and Timing Loop

LabView was used to implement the control loop for the actuators. The timing loop, shown in Figure D-2, was designed so that the actual angle of the rotors could be compared with the desired angle and compensator would adjust the output current. The Graphical User Interface (GUI) is shown in Figure D-1.

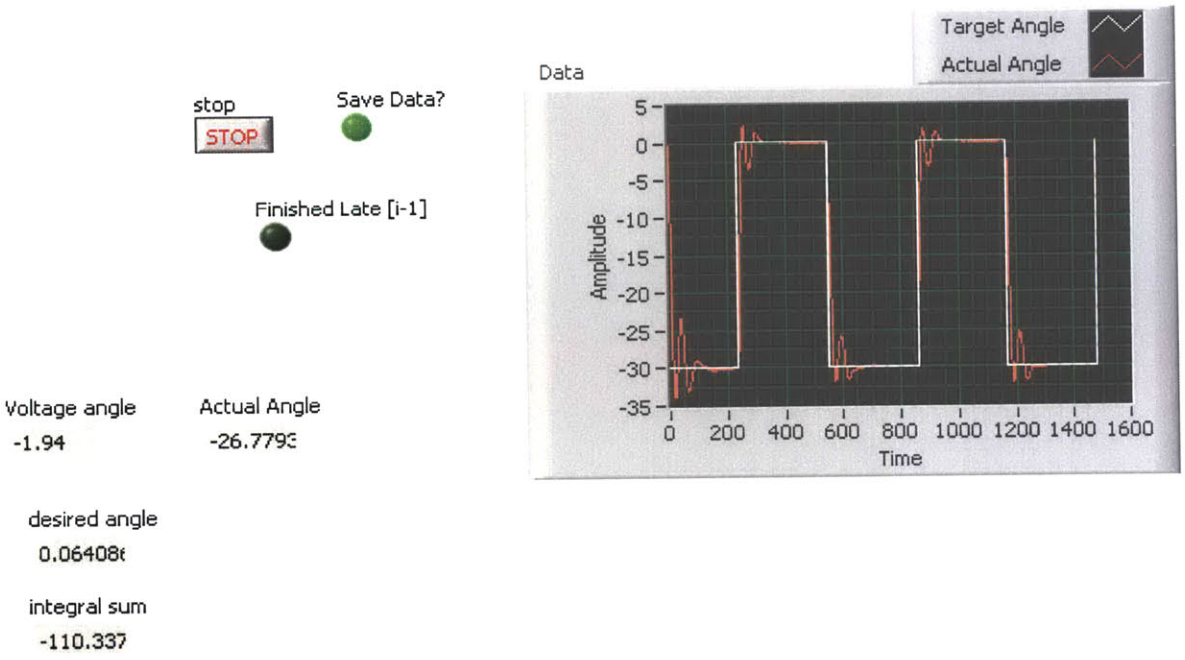

Figure D- 1. Graphical User Interface for LabView PID controller.

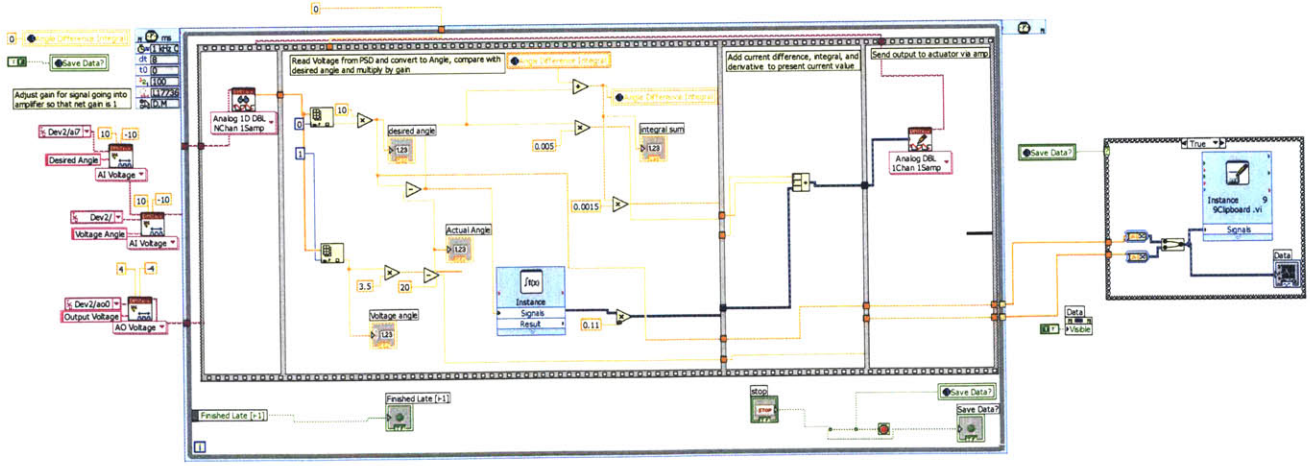

Figure D- 2. LabView timing loop for PID control loop.